AN EXPERIMENTAL INVESTIGATION ON FOCUSSING OF WEAK SHOCK WAVES IN AIR

Thesis by

Vijay Anand Kulkarny

In Partial Fulfillment of the Requirements

For the Degree of

Doctor of Philosophy

California Institute of Technology

Pasadena, California

1975

(Submitted March 14, 1975)

ACKNOWLEDGEMENTS

In the present research, the guidance of Professor Bradford Sturtevant has been most valuable. His interest and insight have had a deep influence on the work, and his constructive criticism is responsible for a great many improvements in the manuscript. His advice and encouragement are sincerely appreciated.

The author wishes to thank Professor G. B. Whitham, Professor J. B. Keller and Dr. Erik Storm; personal discussions with them were very helpful in understanding the phenomena under investigation.

It is a pleasure to thank Mrs. Karen Cheetham for her excellent typing and Mrs. Betty Wood for her beautiful drawings. Special thanks for their patience with the author's shortcomings in these areas during the hectic preparation of this manuscript.

The author is indebted to the California Institute of Technology and the Air Force Office of Scientific Research for their financial assistance. The work in the GALCIT 17-inch shock tube was supported by the Air Force Office of Scientific Research.

ABSTRACT

The behavior of focussing weak shock waves is experimentally investigated with a view to observe and understand the processes occurring near the focus, especially the processes that control the maximum amplitude. Concave reflectors are used against the endwall of a large 17" diameter shock tube, to focus the plane incident shock. Reflectors producing line and point foci, and cusped and smooth caustics are examined for incident shock Mach numbers ranging between 1.005 to 1.5. The flowfield is observed with spark shadowgraphs to visualize the motion of various wavefronts. Pressure histories measured at various points in the flow with miniature piezoelectric gauges provide additional information about the various processes occurring near the focus.

Shadowgraphs show that for weak shocks, the observed foci are predominantly nonlinear, even though away from the focus, the shockfronts appear to be almost acoustic. Thus a weak shockfront, after the focus, crosses itself and forms a loop, which is an essential feature of acoustic wavefronts. Nonetheless, at the focus, distortion in the geometry of the fronts due to nonlinear effects is very prominent. Inherently nonlinear phenomena, such as formation of three-shock intersections, lead to foci of finite size, in which, as the pressure measurements show, the amplitudes are finite.

The amplitude dependence of these phenomena confirms that they are basically nonlinear. The geometrical distortion and the focus are larger for stronger shock waves, and the maximum amplification is smaller. Further, when the distortion becomes significant

compared to the size of the initial shockfront, a transition occurs in the geometry of the focussed shockfront. In this case, the focussed front does not cross and remains "unlooped", which is consistent with the nonlinear behavior predicted by shock dynamics.

The transition in the geometry of the wavefronts is related to the behavior of the three-shock intersections formed near the focus. In fact, it is shown that the occurrence of crossed or uncrossed shockfronts is very parallel to the occurrence of regular or Mach reflection, respectively, in the case of a shock diffracted by a wedge. (The reflecting wedge surface corresponds to the axis of symmetry in a focussing process.) The dependence on the steepness of the approaching waves is also similar in the two cases; rapid convergence of waves suppresses nonlinear effects, whereas in a slow convergence, nonlinear effects gain prominence.

The pressure histories at various locations, when correlated with the waves occurring there, show that nonlinear diffraction processes are very important. In fact, it is shown that the formation of the three-shock intersection occurs due to nonlinear distortion and breaking of a compressive diffraction, and that, in the focus, the limiting and reduction of the peak amplitude occurs by a diffracted expansion overtaking the shock due to nonlinear effects.

TABLE OF CONTENTS

TABLE OF CONTENTS (cont.)

LIST OF FIGURES

LIST OF FIGURES (cont.)

I. INTRODUCTION

A weak shock wave becomes concave towards its direction of propagation in a manner similar to that of a wavefront of sound, by refraction through inhomogeneous or moving media, or by reflection from concave surfaces, or because accelerating supersonic sources generate such curved wavefronts. Whatever the reason, the concave wavefront, once formed, will converge as it travels, and will tend to focus. Consequently, the wave amplitudes will be greatly magnified in the vicinity of the focus. It then becomes important to know the maximum amplitude, in a given situation, and the mechanisms that control this amplitude near the focus.

The prime example of this situation is the focussing of sonic-booms. Refraction through atmospheric thermal inhomogeneities, windfields, or turbulence; reflections from valleys or buildings; or maneuvers of supersonic aircraft are known to cause "superbooms", or intense sonic-booms due to focussing. Even though a major part of the interest in the focussing of weak shock waves comes from sonic-boom problems, the phenomenon is more general and may occur in a variety of problems involving shock waves or supersonic flows, over a vast range of physical scales. The study of the physical processes that limit the maximum amplitudes at a focus is, therefore, of fundamental importance.

As a first approximation, geometrical acoustics can be used to understand the behavior of a focussing weak shock wave (Keller, 1954). If the shock is considered to have a small amplitude and no thickness, it can be identified with the wavefront of a sound pulse. The focussing

of such a shock wave is shown in Fig. 1. The heavy lines show the shock moving to the right, at successive instants. The shock propagates normal to itself with a fixed speed at all times. The trajectories of points on the shock, or rays, are therefore straight lines normal to the shockfront. The rays of a concave shockfront cross as shown by the light lines. The surface on which adjacent rays cross is called a "caustic" surface, shown here by a dotted line. In many cases, the shockfront has a minimum radius of curvature, which leads to a cusp in the caustic, called "arete", also shown here. According to geometrical acoustics, the wave energy contained in a tube of rays remains confined to the tube and when the wavefront comes to a ray crossing, the vanishing cross-sectional area of the tube leads to infinite energy flux and infinite amplitude. Thus geometrical acoustics predicts infinite shock amplitude at the caustic. Evidently geometrical acoustics is not valid near such singular regions because it assumes small amplitudes to begin with.

Nonetheless, geometrical acoustics provides the simplest description of the geometry of the initial wavefront and, to some extent, of the process of focussing. In this work, we use the concepts of geometrical acoustics to describe reflectors and different focussing situations associated with them; the terms focus and focussing have been used in generality, to refer to any such singularity predicted by geometrical acoustics. The degenerate cases of caustics in which infinitely many rays cross at a point or a line are called "perfect foci".

Physically, a shock wave cannot be infinitely thin, but must have the thickness of at least a few mean free paths. Clearly, any

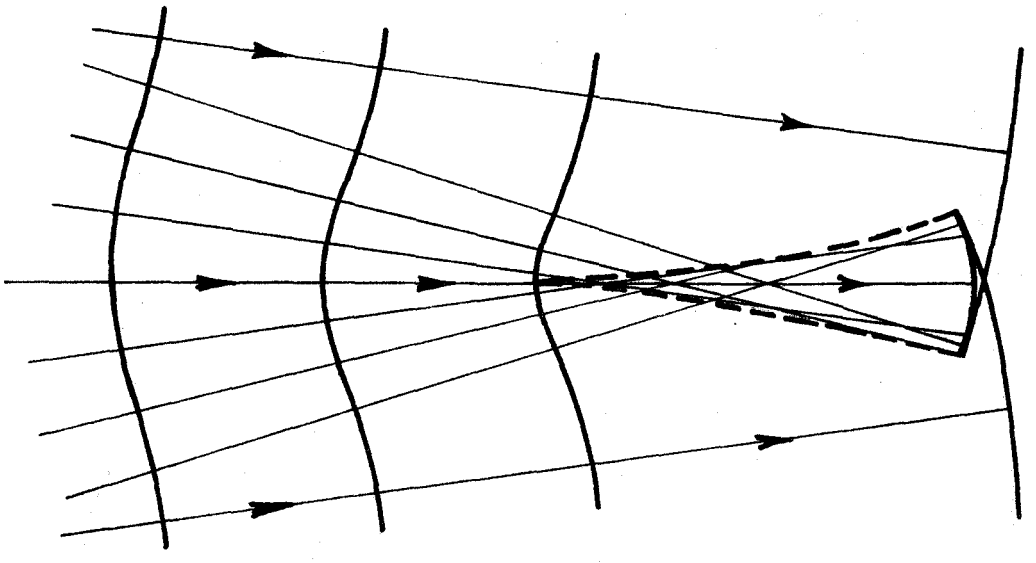

FIG. 1 FOCUSSING OF A SOUND PULSE

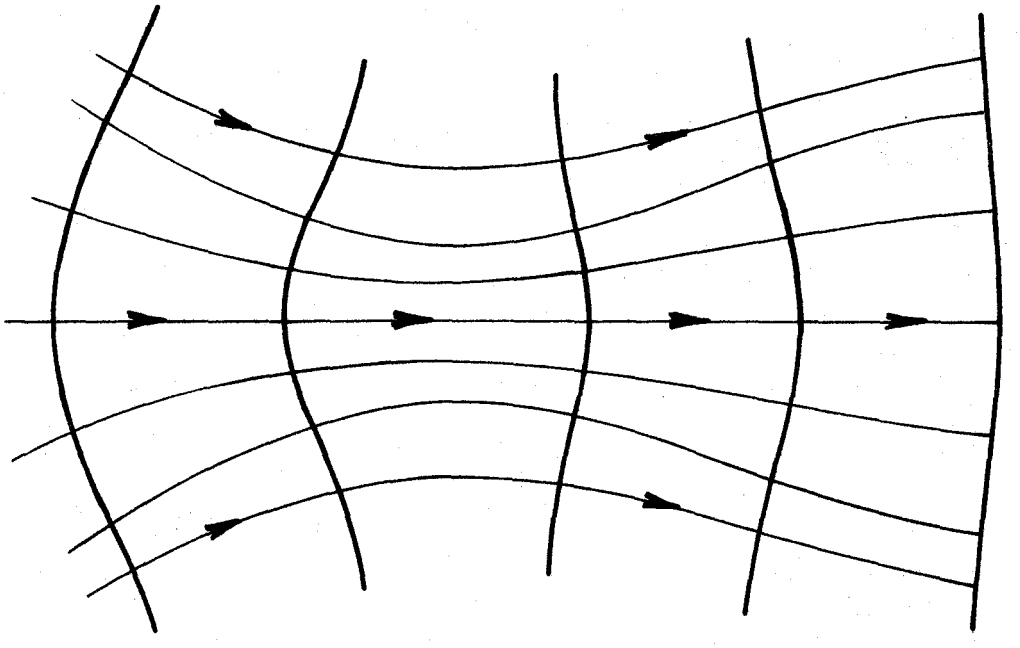

FIG. 2 FOCUSSING OF A STRONG SHOCK

focus of such a shock will also be diffuse to the same extent and will have finite maximum amplitude. 'Physical' or 'wave' acoustics can arrive at this result more rigorously, still assuming shocks of small amplitude, but now with finite thickness. A picture of such focussing would again look identical to Fig. 1, if the line thickness were taken to represent the shock thickness. The reason for this is the invariance of wave speed with amplitude, which is a consequence of the assumption of small amplitude. An essential feature of this kind of focussing is the crossing and folding of the weak shock to form a "loop" as it comes out of the focus (see final shockfront in the figure). Even though this thick-shock picture predicts no singularities, in most situations the shock thickness and the resultant size of the focus are microscopic. This leads to amplitudes large enough to invalidate the assumption of small amplitude, locally near the focus.

The major influence of "finite" amplitudes is the increase in wave speed with amplitude. In fact, it is this manifestation of nonlinearity that leads to shock waves. It would be expected to influence the focussing process also, as the amplitudes become larger, and is taken into account by Whitham's approach to shock dynamics (Whitham, 1957, 1959). In this case, a description similar to geometrical acoustics is used, with shockfronts, and with rays orthogonal to the fronts. However, the shockfront can travel at different speeds along different rays depending on its amplitude. This effect turns the shockfront and bends the rays. Variation of the amplitude of each shock element, as it travels in a curved raytube, is then approximated by the variation in the strength of a plane shock traveling down a

straight tube of slowly varying cross-section. This modified shock strength determines the speeds for traveling along different rays and results in further modification of the shockfront. This cyclic process goes on. Qualitatively, the result of these nonlinear effects on a focussing strong shock may be described as follows (Whitham, 1957). The concave portion of the shock amplifies and accelerates relative to the not-so-concave portions of the shockfront. The rays then curve away from the focus and the shockfront becomes "smooth". This is illustrated in Fig. 2. During such a process, the rays do not cross and the amplitudes are finite. Also, the strong shock comes out flattened, to some extent and unlike a weak shock, it has no loop. (In this study, the term "strong" is only relative; generally $M < 2$.)

Thus it is clear that the nonlinear effects of finite amplitude distort the wavefront-ray geometry progressively. In fact, for strong shocks the final shockfront may appear quite different. However, this does not imply that only when the shockfront comes out with no loop, the focussing is nonlinear, and otherwise it is acoustic. In fact this investigation aims to show that even very minor distortions of the shockfront lead to nonlinear foci. In other words, despite the fact that away from the focus, the shockfronts look very much like the crossed and folded wavefronts of acoustics, at the focus itself nonlinear diffraction processes dominate and determine the maximum amplitude, in most cases of shock-focussing.

1.1 Classification of Foci

Focussing of weak shock waves occurs in practice under many different circumstances. Some typical situations are shown in Figs.

3 to 6. For simplicity, only bow shocks of supersonic bodies are shown and their behavior is indicated with rays drawn according to geometrical acoustics. Also, the figures are only two-dimensional, whereas, in reality, a focussing situation occurs in three dimensions.

A burst of longitudinal acceleration of a supersonic body produces a focus as shown in Fig. 3. In order to keep the geometry simple, a perfect focus is shown, even though, in practice, a caustic with a cusp is more probable. The situation appears almost identical when the supersonic body passes through a longitudinal thermal gradient in the atmosphere, and arrives in a region where the speed of sound is lower. This again amounts to an increase in the Mach number of the body, and is, effectively, an acceleration.

A lateral thermal gradient can produce a different wave pattern traveling along a caustic (Fig. 4). The rays in this case are curved by refraction through the inhomogeneity. The continuous curving turns the rays around giving total internal reflection. Adjacent rays cross when they turn around, forming a caustic there. There is no distinct wavefront traveling with this wave pattern below the caustic, even though there may be an "evanescent" wave. This phenomenon is called "sonic cut off".

Lateral accelerations of the supersonic body can produce situations similar to both of those described above. A lateral acceleration implies a curved trajectory and similarly curved shock waves. Fig. 5 shows a turn maneuver producing a shock with a cusped caustic. On the other hand, a continuous turn in a circle produces a caustic as shown in Fig. 6. Comparing this case with the "sonic cut off", the

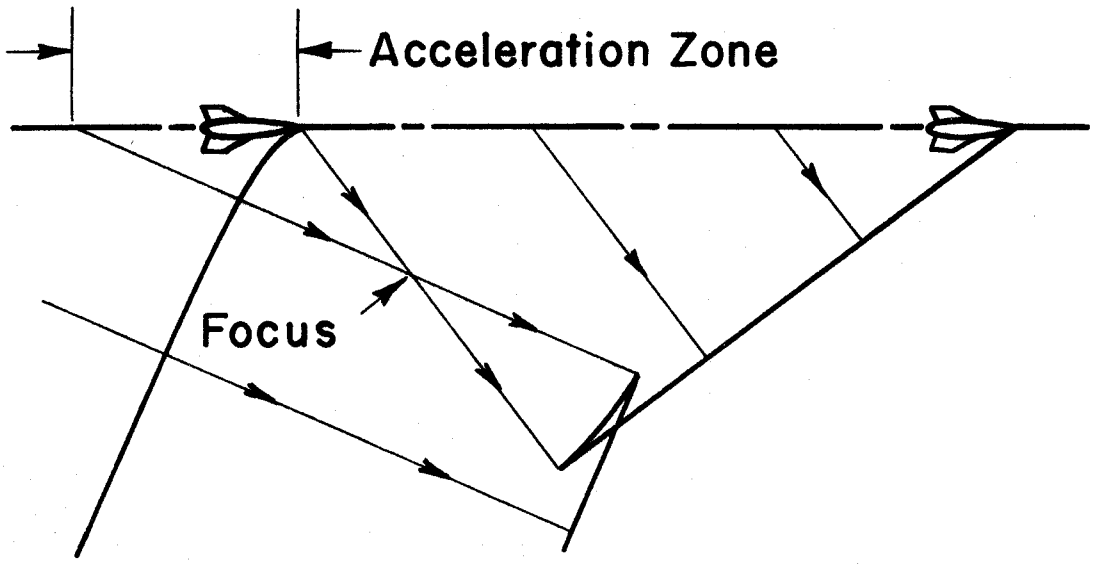

FIG. 3 EFFECT OF ACCELERATION

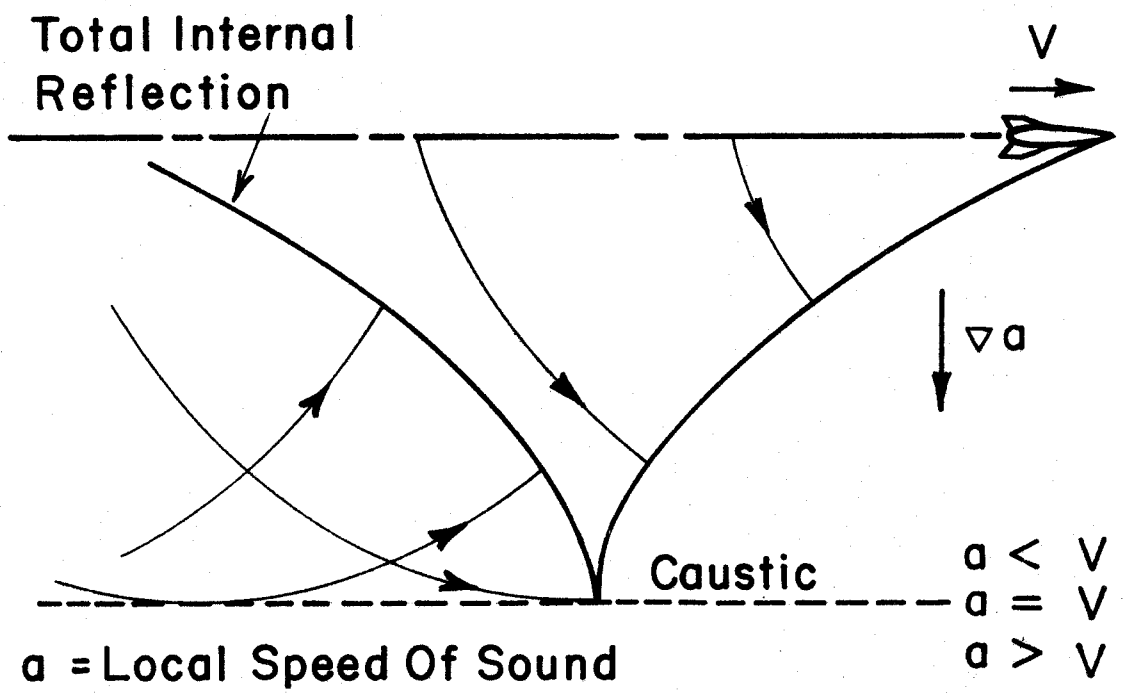

FIG. 4 SONIC CUT OFF

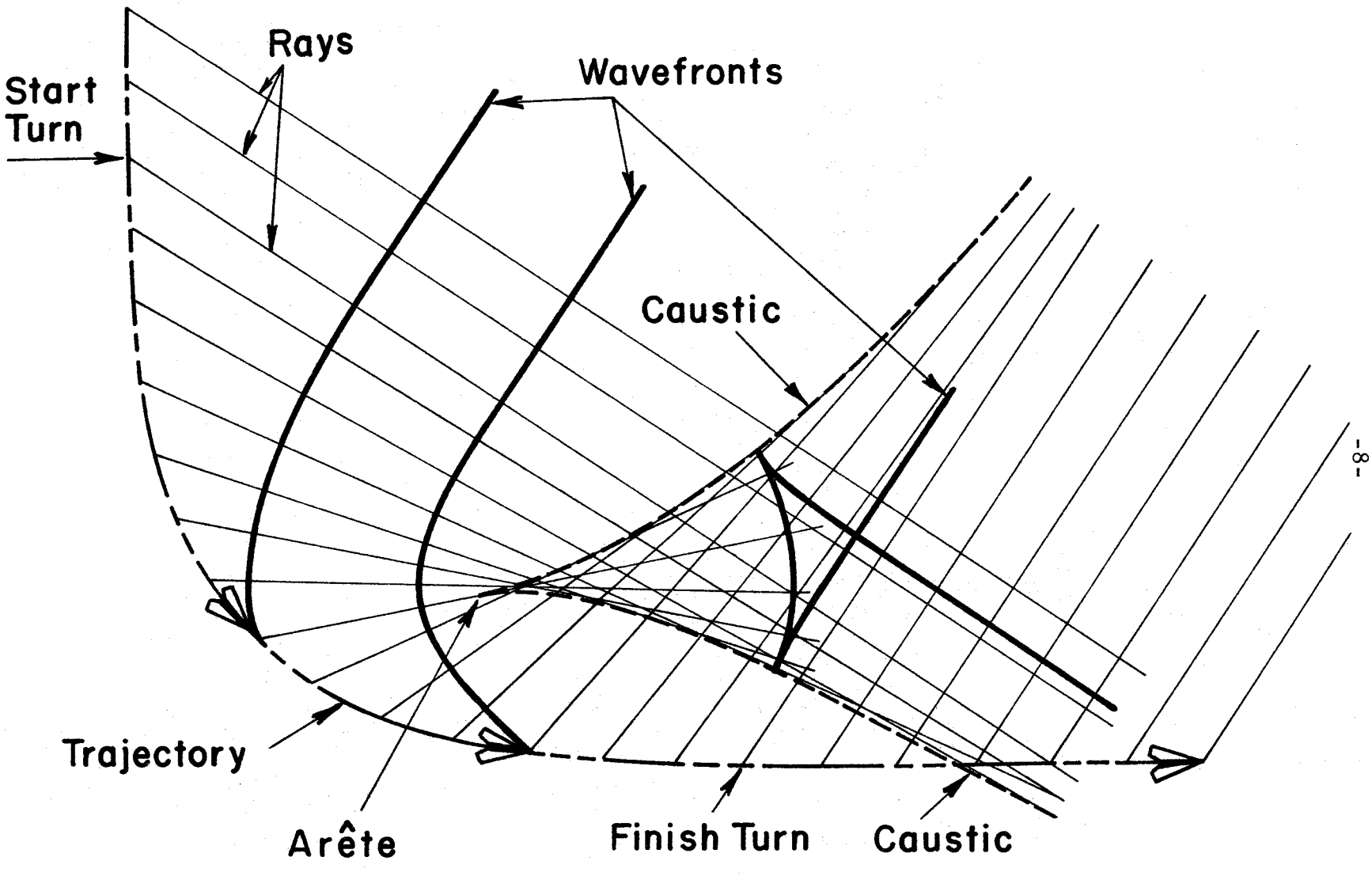

FIG. 5 EFFECT OF A TURN MANEUVER

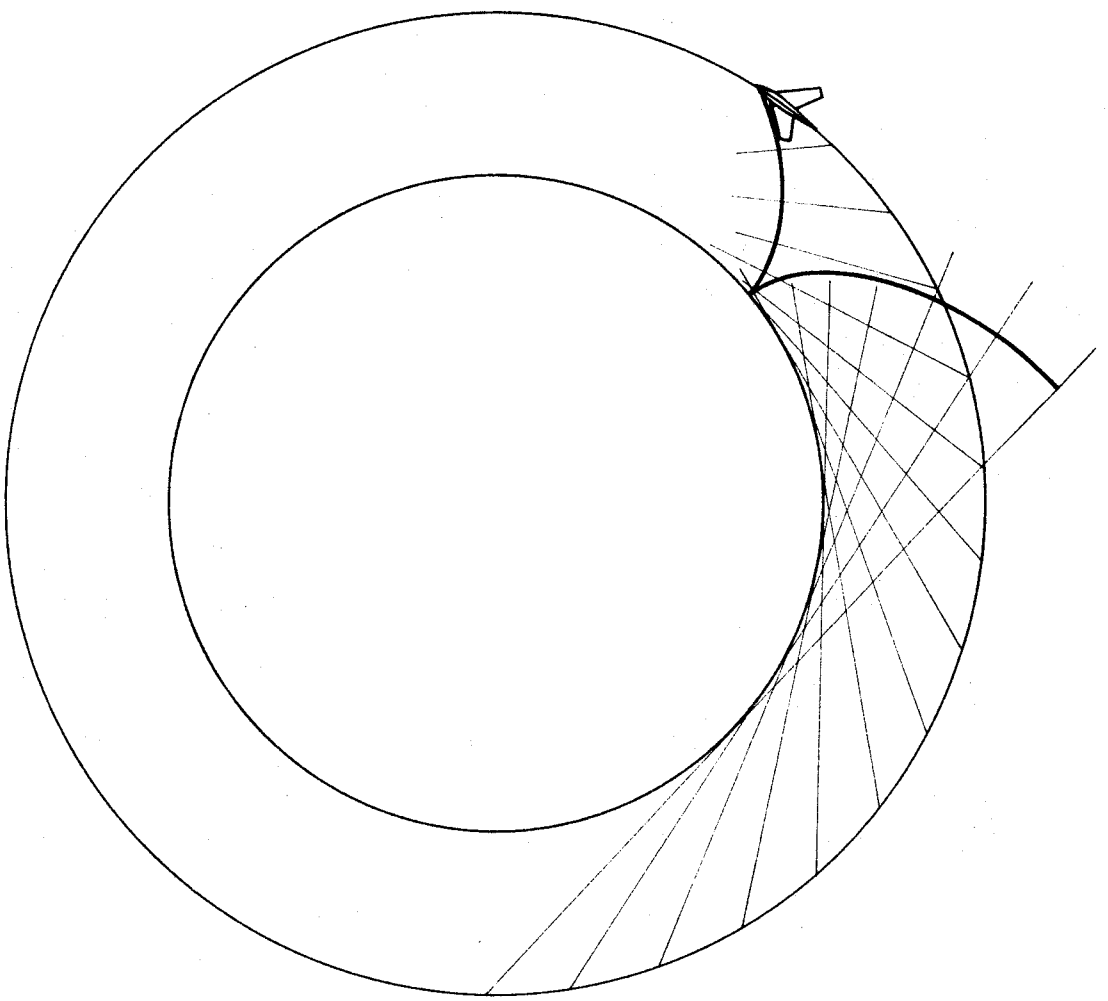

FIG. 6 EFFECT OF A CONTINUOUS TURN

rays here are straight and the caustic has an opposite curvature. The parameter of importance is likely to be, however, the relative curvature between the caustic and the rays, in which case the two caustics are not very different.

At this point, it is possible to distinguish between steady and nonsteady phenomena. In a steady phenomenon, the wavefronts do not change with time. This occurs for both cases of caustics shown here (Fig. 4, 6), when the frame of reference is chosen to move with the supersonic body. For this to occur, the curvatures of the rays and the caustic have to be constant. This cannot happen at the cusp of a caustic because the curvature changes sign there. Therefore, an arete is inherently nonsteady. Similarly, the starting of a caustic is always a nonsteady phenomenon, similar to the cusp of a caustic, in that it produces crossed and folded wavefronts. The cusp, however, is not real, but is simply a point at which the caustic begins, and the other branch of the cusp is not a caustic but a ray on which the wavefront folds. (Such rays occur at a perfect focus also, for example in Fig. 3.) After a long time, this fold and the crossing have moved away from the caustic, and it may be considered as steady, if the curvatures of the caustic and the rays remain constant.

From all these situations of focussing, three kinds of foci may be identified: caustics, aretes and perfect foci. In mathematical terms, the radius of curvature of the traveling shockfront can be expressed as a function of arclength s along the shock and of time t as

$$R(s, t) = R(s, o) - ct \qquad (1)$$

where c is the speed of the shockfront. Then,

(i) $R(s, t) = 0$ implies a caustic,

(ii) $R(s, t) = \frac{\partial}{\partial s} R(s, t) = 0$ implies an arete, and

(iii) $R(s, t) \equiv 0$ for all s in some nonzero range of s implies a perfect focus.

(By definition each class is a subclass of the previous class, but in use the names generally imply exclusion of the subclasses.)

If there are no singularities on the initial shockfront ($R(s, o) \neq 0$ for all s), then it is clear that a local minimum of R leads to an arete. A starting point of a caustic or a perfect focus are rather special circumstances. For a caustic to have an endpoint, R must be discontinuous on the ray passing through the endpoint. The wavefront will fold on this ray, past the caustic, without becoming singular. In this sense, the perfect focus of Fig. 3 is a caustic shrunk to a point, and corresponds to two superposed endpoints. Thus it has two such rays on which R is discontinuous. (R may be continuous, in which case, there are also caustics attached to the perfect focus.) However, under most normal circumstances, R would be a smooth, continuous function of s with a minimum. For example, a large plane shockfront will be locally dimpled when it interacts with a small inhomogeneity, and will lead to an arete as in Fig. 1. On the other hand, the steady caustics are different. The waves, in this case, have "forgotten" the initial shockfront and, for all practical purposes, have always had a singular point at the caustic. The minimum of R is, now, negative infinity, which is reached only asymptotically by the reflected shockfront.

1.2 Acoustics of Focussing Weak Shocks

Acoustics, as used here, is restricted to the description of

pressure waves of small amplitude. Even though its validity may be questioned near a focus, it gives valuable information about the wave field and the processes occurring behind a focussing weak shock. This section summarizes some relevant results from acoustics that would be useful in analyzing the focussing of weak shock waves.

The assumption of small amplitudes (or perturbations) allows linearization of the equations of irrotational motion in an inviscid, homogeneous isotropic fluid, and leads to the wave equation for sound in the fluid:

$$\nabla^2 \phi - \frac{1}{c^2}\phi_{tt} = 0 \; ; \qquad c = \left(\frac{\partial p}{\partial \rho}\right)_s \tag{2}$$

where ϕ is the velocity potential, p is the fluid pressure, ρ is the fluid density and s is the entropy of the fluid. Shocks with their entropy jumps can fit into this isentropic description because the entropy change is of third order in terms of the pressure change and may be neglected for small amplitude waves. This hyperbolic partial differential equation has characteristics in space-time described by the eikonal equation:

$$\nabla S . \nabla S - \frac{1}{c^2} S_t^2 = 0 \tag{3}$$

where $S(\bar{x}, t)$ = constant is a characteristic surface in space-time. For changing values of t, the surface S describes a wavefront, which moves normal to itself with a speed c. The eikonal equation also has characteristics, which are curves on S and whose projections on space are rays (Friedlander, 1958). The rays are normal to the wavefronts in an isotropic medium and they are straight lines in a homogeneous medium.

1.2a Geometrical Acoustics

It can be shown that weak shock waves, which may be treated as discontinuous, "weak" solutions of the wave equation, can occur only along its characteristics (Whitham, 1974). (More simply, this occurs because initial values may be specified independently across the characteristics. Linear hyperbolic partial differential equations reduce to ordinary differential equations along the characteristics. Thus the solution can take different values across the characteristics, but will be continuous along them.) In the geometry of wavefronts and rays, this identifies shockfronts with wavefronts. Given a shockfront, then, its position and shape at later times can be found by drawing rays normal to the front and advancing the front by an appropriate distance along the rays. In the presence of boundaries, reflected fronts can be constructed consistent with the laws of reflection (Friedlander, 1958).

This behavior is closely paralleled by light waves, because electromagnetic fields also obey the wave equation (where c represents the speed of light). However, in this case, there are high frequency sinusoidal waves, instead of discontinuities. Again in the asymptotic approximation of infinite frequency, the "phasefronts" or the surfaces of constant phase coincide with the wavefronts and behave similarly (Keller, 1954; Friedrichs and Keller, 1956). This parallel between high frequency sinusoids and discontinuities is not unexpected as they are related by Fourier analysis of discontinuous functions. Also, this behavior of wavefronts, shockfronts and phasefronts agrees with both Fermat's Principle and Huygen's construction.

The amplitude of the shock or of the high frequency sinusoidal

waves at later times can be found with the "transport equation", obtained from the wave equation by approximation after substituting an assumed form for the solution (Whitham, 1974). For a shock,

$$2\nabla S \cdot \nabla\phi_1 + (\nabla^2 S - \frac{1}{c^2} S_{tt})\phi_1 = 0 \; ; \qquad \phi = H(S) \sum_{n=1}^{\infty} \phi_n \frac{S^n}{n!} \qquad (4)$$

where H(S) is the Heaviside Step Function. The transport equation has the same characteristic curves as the eikonal equation (Whitham, 1974). Therefore discontinuities of shock amplitude, proportional to ϕ_1, may occur across the rays for the same reason that shocks could occur along the characteristics of a wave equation. For infinite frequency sinusoidal waves, or for shockfronts, this corresponds to sharp shadows. Further, the transport equation can be integrated to show that the amplitude in a narrow ray tube varies inversely proportional as the square root of the area of cross section of the ray tube. This can be loosely interpreted as a form of conservation of wave energy, as the energy is proportional to the square of the amplitude (Keller, 1954; Freidrichs and Keller, 1956).

Thus, the behavior of a shockfront or a phasefront can be determined in part, simply by geometrical considerations of the initial front. This "geometrical acoustics", however, is valid only in the asymptotic approximation of strict discontinuities and infinite frequencies (or zero wavelengths), and does not give the complete solution to the wave equation. It excludes shocks of finite thickness, or waves of finite frequency, and says little about the pressure field behind the shock (Keller, 1954; Friedrichs and Keller, 1956). Also, near a focus the cross-sectional area of the ray tube vanishes, and the amplitude

becomes infinite according to geometrical acoustics. Thus the amplitudes at and beyond the focus cannot be found, though the shockfronts can be. To solve these problems a more complete solution of the wave equation is necessary.

1.2b Poisson's Solution

In homogeneous media without any interfering boundaries, a solution of the wave equation (1) is given by Poisson in terms of averages of initial distributions of amplitude, ϕ^o, and its time derivative, ϕ_t^o. The averaging is done over the surface of a sphere of radius c t centered at the point of interest $\bar{x}$. If such an average is represented as a functional $M(\phi)$, the solution can be written as follows (Whitham, 1974).

$$\phi(\bar{x}, t) = \frac{\partial}{\partial t}\left[c t M(\phi^o)\right] + c t M(\phi_t^o) \qquad (5)$$

Unlike geometrical acoustics which computes shock amplitude from point to point along rays, this form of the solution connects the amplitude at any point and time directly to the initial values, irrespective of the amplitudes in between. Therefore this solution can be used to evaluate some amplitudes beyond a focus. But, so far as the shocks have no thickness, it predicts infinities at the foci and on certain shockfronts coming out of the focus (Friedlander, 1958). According to this solution, a shockfront, when it passes through a line focus, not only becomes infinite in amplitude, but changes into a logarithmic compression-expansion front. Furthermore, if the curvature in the other direction focusses this front again then it comes out as an expansion shock. In the case of a point focus, both curvatures become

infinite at the same time and the shock skips the intermediate stage of the logarithmic front. This is illustrated in Fig. 7, for a perfect focus.

Poisson's solution can also deal with thick shocks and finite frequencies, and it can predict the pressure field behind the shock, but the answers are not very explicit as they depend on details of the averaging. In an unobstructed, homogeneous, isotropic medium, it confirms and supplements the answers of geometrical acoustics.

1.2 c Diffraction

Geometrical acoustics, being an approximation, does not give all the wavefronts. It predicts regions of sharp shadow, whereas in practice, wavefronts and rays do occur in such regions. These new wavefronts and rays can be described with Fermat's Principle or Huygen's Construction. Also, wave-like variations of amplitude may be observed in the flow behind curved shock waves. Such waves are the result of a phenomenon called "diffraction".

Geometrical acoustics tolerates discontinuous amplitudes across rays (as explained previously). But this is true only at the shock itself, or in the limit of infinite frequency only. Such a discontinuity in the amplitude of the shock leaves discontinuities in the pressure field behind the shock. These discontinuities of pressure will drive waves until the pressure becomes uniform everywhere. These waves are the diffraction waves. Examples of such wave fields can be found in diffraction of sound pulses by wedges (Friedlander, 1958).

The instant a discontinuity in pressure occurs along the shock-front, a front of the diffraction wavefield starts and travels radially

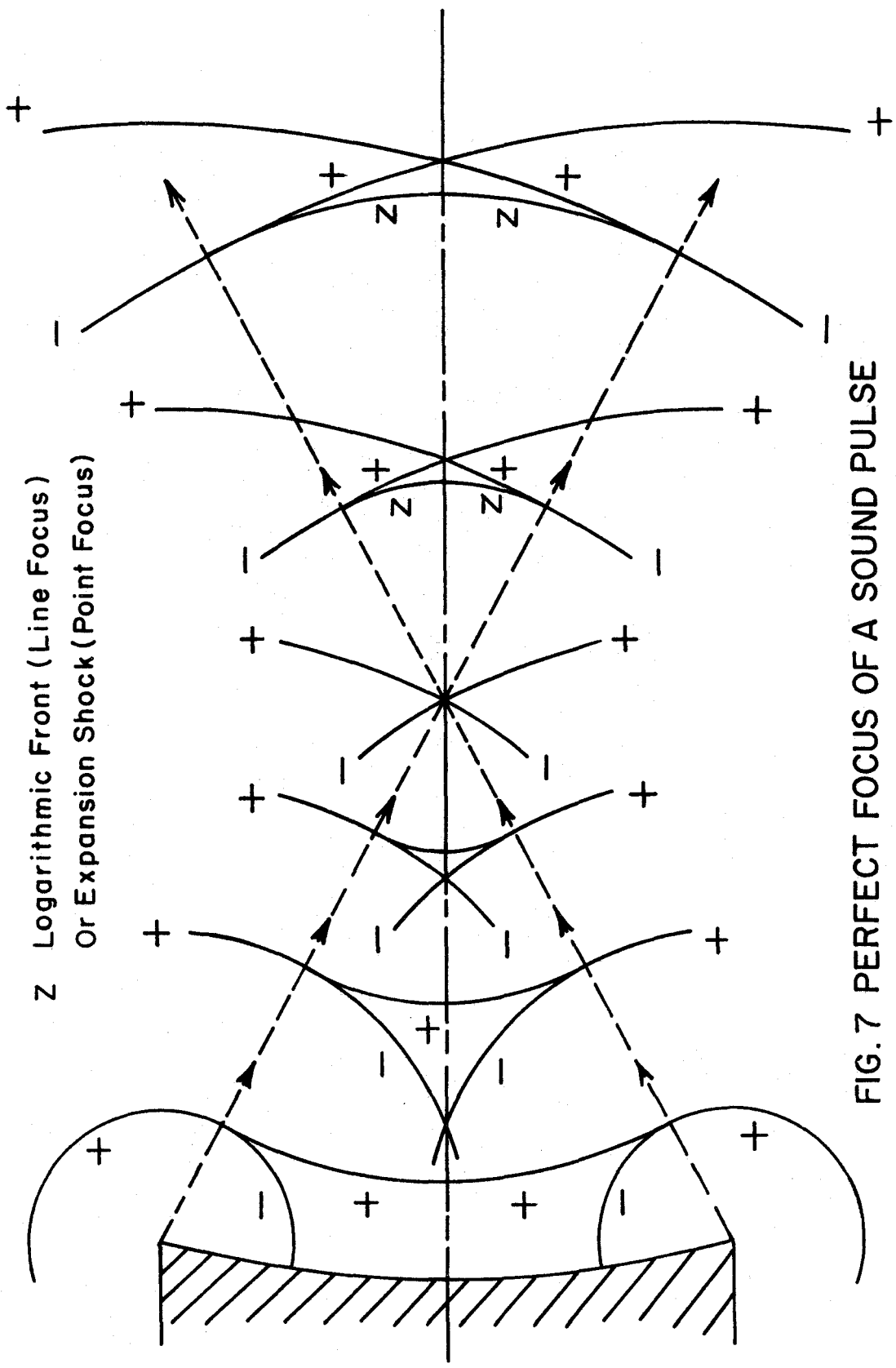

FIG. 7 PERFECT FOCUS OF A SOUND PULSE

out from that point with the speed of sound. The front is generally not a shock, but a more gradual pressure change (Keller, 1954; Friedrichs and Keller, 1956). The portion traveling into the high pressure fluid is an expansion and the portion traveling into the low pressure fluid is a compression. The net effect is to bring the fluid to some intermediate equilibrium pressure. Fig. 7 shows such diffraction fronts spreading from sharp edges of the reflector. The discontinuity in amplitude at the shock continues to travel along. However, the pressure distribution immediately behind the discontinuity becomes smooth, continuous and settles to the mean pressure. At other points on the diffracted front, away from the discontinuity, the pressure change begins as the square root of time. Later, far behind the diffracted front, the pressure everywhere smoothly settles down to the same final equilibrium pressure. All diffractions which result from discontinuities in the amplitude of the shock have this character. Clearly, if the curvature of the shock is discontinuous across a ray, a growing discontinuity in shock amplitude results along this ray, followed by a diffraction wavefield. This occurs for all cases of perfect focus and is shown in Fig. 7.

For aretes and caustics, the curvature of the shock and therefore its amplitude change continuously along the shockfront. Thus there are no discontinuities, but pressure gradients are created nonetheless. Evidently there can be no distinct diffraction fronts, but the pressure gradients set up a wavefield to bring the fluid to an equilibrium pressure. Even though the diffraction waves are not distinct, they still must have the same character: expansions traveling into the

high pressure fluid and compressions into the low pressure fluid.

In general, variations along the shockfront create nonuniform pressures behind the shock, which relax to a uniform equilibrium pressure by generating diffraction waves behind the shock. In the acoustic approximation, these waves travel with the same speed as the shock. If the shock is thick, then near a focus, its crest is affected by diffraction waves within a region of the size of the shock thickness, and the amplitudes are finite. (Similar effects occur for high frequency periodic waves. Further, the phasefronts of these waves become locally plane in the focus (Debye, 1909; Kay and Keller, 1954).) On the other hand, if the shock has no thickness, the diffraction waves cannot affect the shockfront. Therefore, the singularities predicted by geometrical acoustics remain, so far as the shock is treated as having no thickness. Under these circumstances, the amplitudes clearly depart from infinitesimal, and other amplitude-dependent phenomena enter the picture. This is discussed in the next section.

1.3 Dynamics of Shock Waves

It is well known in fluid flows that when wave amplitudes become finite, the increase in wave velocity becomes significant. If an acoustic approximation is used, the error in the slopes of the characteristics increases with amplitude. The total error grows with time or distance traveled (Friedlander, 1958; Whitham, 1974). This gives the familiar distortion of waveforms, which break to form shock waves.

Thus a shock wave is continually overtaken and modified by the wavefield behind it. The velocity of the shock wave is approximately

the mean of the wave velocity ahead of it and the wave velocity behind it, especially for a weak shock. The shock velocity also, therefore, increases with amplitude (Whitham, 1974).

Shock dynamics is an approximate theory, developed by Whitham, to predict the motion of such nonlinear shockfronts in two or three dimensions (Whitham, 1957, 1959, 1974). It applies in situations where the nonlinear interaction occurs mainly between the shock and the geometry, and the interaction with the wave field behind the shock is weak (Whitham, 1974). (In contrast to this, an acoustic shock is free of any interaction with the wave field behind it.)

In this approach, using the fact that a shock travels normal to itself, rays are introduced as orthogonal curves to the shockfront. The shock travels with different speeds along different rays, depending on its local amplitude. Therefore gradients in amplitude and speed turn the shockfront as it travels. Consequently, rays curve away from regions of large amplitude. The variation in shock strength due to ray convergence or divergence is approximated with the shock strength variation of a plane shock traveling in a straight tube of slowly varying cross section. The approximation neglects the cummulative effect of area changes on the wave field behind the shock. Also, particle paths behind the shock are assumed to lie along the rays, although, in actuality, they may deviate from them after the passage of the shock (Whitham, 1974).

It turns out that the system of partial differential equations describing this kind of shock motion is hyperbolic, and disturbances propagate as waves along the shockfront. The waves carry changes in

slope and Mach number M of the shock with a wave speed which is an increasing function of M. These waves on the shock can generally be identified with some wave (known to exist from independent considerations) in the flow behind the shock, traveling oblique to the shock and intersecting with the shock. The wave on the shock represents the movement of this intersection along the shock.

The waves on the shock are nonlinear just as the waves behind the shock; therefore, increases in M steepen, whereas decreases in M spread out. This leads to the breaking of the waves carrying increases of M along the shock. The breaking corresponds to a discontinuity in slope and in M. The trace of this "shock" on the shock is called a "shock-shock". Physically, this corresponds to another shock wave intersecting the shockfront obliquely from behind, thus forming a "three-shock" or "Mach intersection".

It should be emphasized that, because rays curve away from regions of large amplitude, the shock becomes concave in a wave carrying an increase in M. Thus shock-shocks and three shock intersections are a natural outcome of a concave shockfront, according to shock dynamics.

Results of calculations of focussing shock waves, using the equations of shock dynamics, are not available. However, some asymptotic cases may be considered. The concave corner in Fig. 8 is an asymptotic case of a concave corner with a small radius. The reflections in the two cases must look similar after a long time. Reflections from a concave corner are shown in Fig. 8, according to both acoustics and shock dynamics (Whitham, 1957, 1959). The

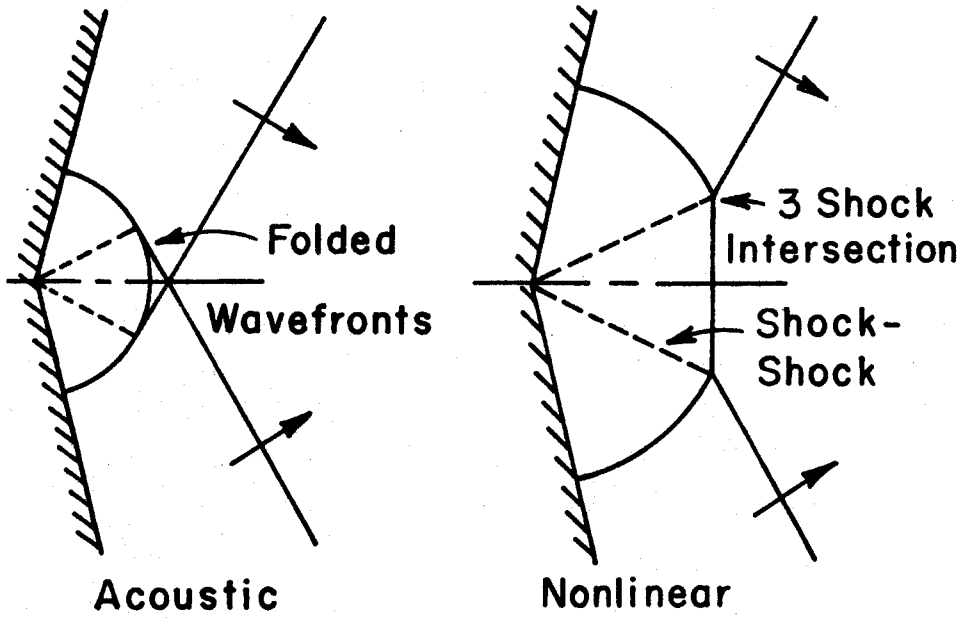

FIG. 8 REFLECTION FROM CONCAVE CORNER

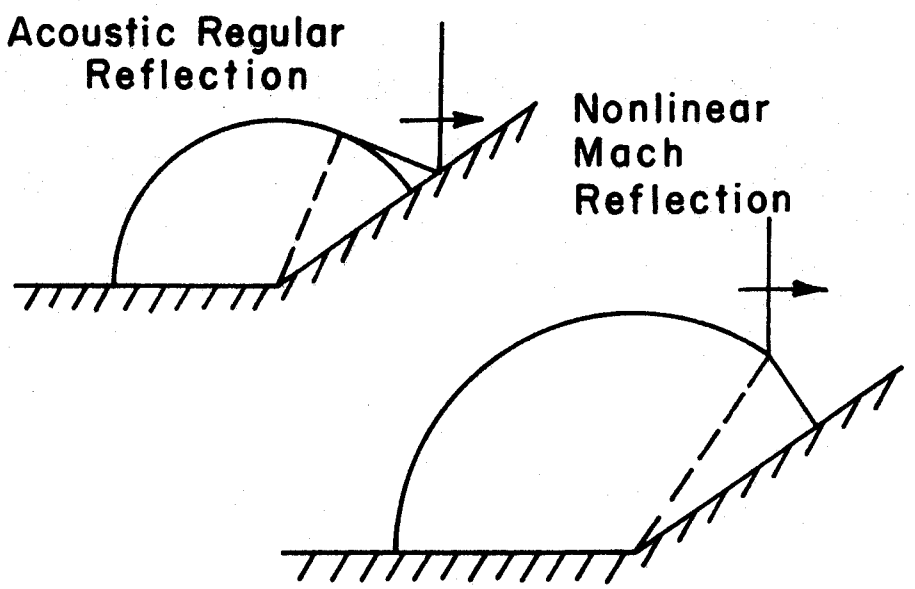

FIG. 9 DIFFRACTION FROM A WEDGE

appearance of a crossed and folded shockfront, and a flattened shockfront, respectively, seem consistent with the behavior of focussing shocks. The case of shock-diffraction from a wedge represents only a half of such a reflection from a shallow concave corner. In this case, it is easier to identify the folded wavefronts with regular reflection and the wavefronts without folds with Mach reflection (Fig. 9). In Fig. 8, these reflections occurred from the axis of symmetry. The occurrence of three-shock intersections in the nonlinear cases is interesting; they are connected with the occurrence or non-occurrence of crosses and loops in the shockfront. This will be seen also from the results of this investigation.

Intuitively, effects similar to Mach reflection should occur for total internal reflections also. For example, near sonic cutoffs (Fig. 4), three-shock intersections have been found to occur instead of the cusps of the shockfronts (Sanai and Toong, 1974). Similar behavior may be expected from cusps of shockfronts near other caustics also (Naumann and Hermanns, 1973). Thus, it appears that the three-shock intersections are important to the behavior of shocks near foci, in general.

Three-shock intersections have been analyzed also by independent and more rigorous approaches (Henderson, 1965). There are many possible three-shock configurations in supersonic flows. Only three of these correspond to Mach reflections (the total deflection of flow through these is small), and are of interest here: direct, stationary and inverted (Courant and Friedrichs, 1948). The direct intersection occurs in a Mach reflection and travels away from the reflecting wall.

The stationary intersection travels parallel to the wall. The inverted intersection, if it occurs at all, travels into the wall, and is replaced by regular reflection. It may therefore, occur only as a transient phenomenon, for example, if the wall turns slowly into the flow until a regular reflection occurs.

In summary, it appears that the nonlinear behavior of focussing shock waves is closely related to the formation and behavior of three-shock intersections, the occurrence of regular or Mach reflection and the corresponding presence or absence of crosses and loops in the shockfronts. In fact, it will be seen that three-shock intersections play a crucial role in determining the behavior of a shock near a focus.

1.4 Previous Investigations

For the purposes of this study, focussing sonic booms may be considered as a pair of focussing shock waves. Then a great volume of measurements is available from field investigations of sonic boom phenomena. Unfortunately, as to the details of any focal processes, the evidence is very inconclusive in most cases. Large uncertainties are introduced by the uncontrolled, random atmosphere, and inferring the flow in the focus with pressure records taken at scattered points becomes difficult. Nonetheless, very good measurements have been made, after extensive investigations, by Wanner et al. (1972), and Haglund and Kane (1974). Their observations show wavefront configurations indicating nearly acoustic focussing.

There have been attempts at simulating the sonic-boom behavior in the laboratory environment, using electric sparks to create N-waves. Beasley et al. (1969), Thery et al. (1970), and

Cornet (1972) have studied the focussing of such weak waves. Except for the very minor wave distortion described by Cornet, no evidence of nonlinearity was observed. The measurements fit the predictions of acoustics very well except near the singularities, where the resolution of the instruments becomes crucial. Evidently, for such weak waves, the distortion created by nonlinear effects within the small scale of the experiments is extremely small. Thus the foci were so minute that they could not be resolved by the methods used.

On the other hand, behavior of strong shocks has been observed in many cases. In an investigation on shock stability, Briscoe and Kovitz (1968) have photographed perturbed shocks. These pictures show shockfronts coming out of foci without any folds. Sturtevant (1973) has reported the preliminary stages of the present investigation where measurements of pressure transients indicated that, in these experiments, folding of the shockfront was prevented by nonlinear effects. Naumann and Hermanns (1973) have observed shockfronts near caustics, during their investigation of the interaction between a shock wave and a vortex field. Here also, the shockfronts have no loops or folds, but they have three-shock intersections. Sanai and Toong produced foci by refraction inside a ballistics range. They found no evidence of folding near aretes. However, they did observe three-shock intersections in their simulation of the sonic cut off (Sanai and Toong, 1974).

On the theoretical side, acoustics and shock dynamics constitute the basis for explaining the focussing of shock waves. Many of the investigations apply or extend these theories to specific cases. For example, by using Poisson's Solution to the wave equation Pierce (1968)

has demonstrated the diffraction waves behind a focussing sonic boom, and Obermeier (1973) has examined the foci of sonic booms with thick shocks, using Fourier integrals. Among the nonlinear theories, Friedman et al. (1963) have extended the shock dynamics theory in order to apply it to focussing by atmospheric refraction. It has been claimed by Friedman (M. P.) and Chou (1965), and independently by Friedman (M. B.) (1968), that their shock dynamic computations fail to show focussing near a sonic cutoff.

On the other hand, for such steady caustics, Guiraud (1965) and Hayes (1968) have speculated a nonlinear similarity behavior near the singular region, based on transonic flow equations. Using these results, Seebass et al. (1970) and Gill (1973) have obtained solutions for the nonlinear behavior of shocks near caustics. Pierce (1971) also has suggested a scaling for the maximum amplitude at an arete. These theories, however, need substantial verification from experiments.

In short, both nearly-acoustic and strongly-nonlinear behaviors of focussing shock waves have been well documented. It is clear that the behavior of focussing shock waves changes with amplitude. In fact, it changes such that the cross and loop on a focussed weak shockfront disappear if the shockfront is strong. However, the previous investigations have not demonstrated how such changes occur. Also, the influence of parameters such as the focal length and the angle of convergence has not been examined. Further, for the nearly-acoustic shocks, no evidence of any amplitude-controlling mechanisms has been observed near the foci. The theories proposing such mechanisms lack

adequate verification, indicating the need for well-defined laboratory investigations under controlled conditions. The present study aims to deal with these problems.

REFERENCES

Beasley, W. D., Brooks, J. D., and Barger, R. L. 1969 A Laboratory Investigation of N-Wave Focussing, NASA TN D-5306.

Briscoe, M. G., and Kovitz, A. A. 1968 Experimental and Theoretical Study of the Stability of Plane Shock Waves Reflected Normally from Perturbed Flat Walls, J. Fluid Mech. 31, 529.

Cornet, E. P. 1972 Focussing of an N-Wave by a Spherical Mirror, Applied Research Labs., University of Texas, ARL-TR-72-40.

Courant, R., and Friedrichs, K. O. 1948 Supersonic Flow and Shock Waves, Interscience, New York.

Debye, P. 1909 Ann. D. Phys. 30, 755. Cf. also Sommerfield, A., 1954 Optics, Academic Press, New York, 318.

Friedlander, F. G. 1958 Sound Pulses, Cambridge University Press.

Friedman, M. B. 1968 Comments on Focusing Due to Atmosphere, NASA SP-180, 115.

Friedman, M. P., Kane, E. J., and Sigalla, A. 1963 Effects of Atmosphere and Aircraft Motion on the Location and Intensity of a Sonic Boom, AIAA Journal 1, 1327.

Friedman, M. P., and Chou, D. C. 1965 Behavior of the Sonic Boom Shock Wave Near the Sonic Cut Off Altitude, NASA CR-358.

Friedrichs, K. O., and Keller, J. B. 1956 Geometrical Acoustics. II., J. Appl. Phys. 26, 961.

REFERENCES (cont.)

Gill, P. M. 1973 Nonlinear Acoustics Behavior at a Caustic, Ph. D. Thesis, Cornell University.

Guiraud, J. P. 1965 Acoustique Geometrique, bruit Ballistique de Avion Supersoniques et Focalisation, J. de Mecanique 4 (2), 215.

Haglund, G. T. and Kane, E. J. 1974 Flight Test Measurements Near the Shock Wave Extremities of Flight Near Mach 1.0 and for Airplane Accelerations, NASA CR-2417.

Hayes, W. D. 1968 Similarity Rules for Nonlinear Acoustic Propagation through a Caustic, NASA SP-180, 165.

Henderson, L. F. 1965 The Three-Shock Confluence on a Simple Wedge Intake, Aero. Quart. 16, 42.

Kay, I. and Keller, J. B. 1954 Asymptotic Evaluation of the Field at a Caustic, J. Appl. Phys. 25, 876.

Keller, J. B. 1954 Geometrical Acoustics. I., J. Appl. Phys. 25, 938.

Naumann, A. and Hermanns, E. 1973 On the Interaction Between a Shock Wave and a Vortex Field, Noise Mechanisms, AGARD CP-131.

Obermeier, F. 1973 Sonic Boom Behavior Near a Caustic, Noise Mechanisms, AGARD CP-131.

Pierce, A. D. 1968 Spikes on Sonic Boom Pressure Waveforms, J. Acoust. Soc. Am. 44, 1052.

Pierce, A. D. 1971 Maximum Overpressures of Sonic Booms Near the Cusps of Caustics, Noise and Vibration Control Engineering,

REFERENCES (cont.)

M. J. Crocker ed., Purdue University Press, 478.

Sanai, M. and Toong, T. Y. 1974 Laboratory Investigation of Sonic Boom Focussing, 2nd Interagency Symp. on U. Research in Transport. Noise, North Carolina State University, Raleigh.

Seebass, R. 1970 Nonlinear Acoustic Behavior at a Caustic, NASA SP-255, 87.

Seebass, R., Murman, E. M. and Krupp, J. A. 1970 A Finite Difference Calculation of the Behavior of an Acoustic Pulse Near a Caustic, NASA SP-255, 361.

Sturtevant, B. 1973 Studies of Shock Focussing and Nonlinear Resonance in Shock Tubes, Recent Developments in Shock Tube Research, Bershader, D. and Griffith, W. Eds., Stanford University Press.

Thery, C., Peter, A. and Pfister, M. 1970 Interaction Entre Bangs et Obstacles. 2 eme partie: Etude de la Reflexion d'un Bang dans un Fond de Vallee, Institut Franco-Allemand de Recherches de Saint Louis, Note Technique - T 9/70.

Wanner, J. -C., Vallee, J., Vivier, C. and Thery, C. 1972 Theoretical and Experimental Studies of the Focus of Sonic Booms, J. Acoust. Soc. Am. 52 (1) 1, 13.

Whitham, G. B. 1957 A New Approach to Problems of Shock Dynamics - Part 1. Two Dimensional Problems, J. Fluid Mech. 2, 145.

REFERENCES (cont.)

Whitham, G. B. 1959 A New Approach to Problems of Shock Dynamics - Part 2. Three Dimensional Problems, J. Fluid Mech. 5, 369.

Whitham, G. B. 1974 Linear and Nonlinear Waves, John Wiley and Son, Inc., New York.

II. EXPERIMENTAL APPARATUS AND PROCEDURE

2.1 The GALCIT Seventeen-inch Shock Tube

The GALCIT 17" diameter shock tube, originally designed for studies of rarefied gases (Liepmann et al., 1962) was used due to its convenient large size, and its high repeatability in producing very plane shock waves. In these experiments, it produced weak shocks in atmospheric air with compressed nitrogen for driver gas. The shock tube has a 12.5' driver and a 70' test section. A set of straight knife blades was used to burst different diaphragms, to obtain well-converged shock waves at the end of the test section. The shock Mach numbers varied from 1.005 to 1.5 as shown in Table 1, with test times ranging between 5 msec for the strongest to 25 msec for the weakest. Also weak shocks made with mylar diaphragms converged much quicker than those made with metal diaphragms. The boundary layer thicknesses are estimated to be less than 1 mm in the region of interest.

2.2 Concave Endwall Reflectors

Cylindrical reflectors were constructed of machined wood blocks, smoothed and repeatedly polished with a sanding sealer to obtain a high finish. Parabolic reflectors, producing perfect line foci, were machined by following templates, whereas more complex shapes producing caustic surfaces and their cusp lines were machined by following coordinates. The wood blocks were fastened to metal plates during machining and during the experiments to reduce the effect of warping.

A paraboloid reflector producing a point focus was also constructed with a commercial glass reflector embedded in epoxy on a wooden backing.

Table 2 lists the various reflectors and their important characteristics.

To locate the reflectors at various distances from the instrument ports in the shock tube, a movable endwall was constructed. This endwall rests on adjustable nylon pressure pads and is supported axially from behind with a large screw which transmits the force on the movable endwall to the shock tube endwall (Fig. 10).

In all geometries of the reflectors, it was necessary to keep the aperture of the reflector sufficiently small so reflections of scattered waves from shock tube walls do not enter the flowfield during the time of measurement. Especially in two-dimensional geometries, such as a cylindrical reflector producing a line focus, it is impossible to avoid this effect completely. Reducing the width of the reflector, however, does restrict it to the lateral ends of the reflector, in which case it would be observed as secondary waves.

2.3 Shadowgraph System

The flowfield of the reflected shock waves was observed with spark shadowgraphs. The spark has a duration of less than a microsecond and freezes the wave pattern very well. It was necessary to use very fast film, and Polaroid Land film type 108 (ASA 3000) was found to be very convenient. The whole system was enclosed in a black box to allow operation in daylight.

As shown in Fig. 12, a Schlieren mirror of 54' focal length was

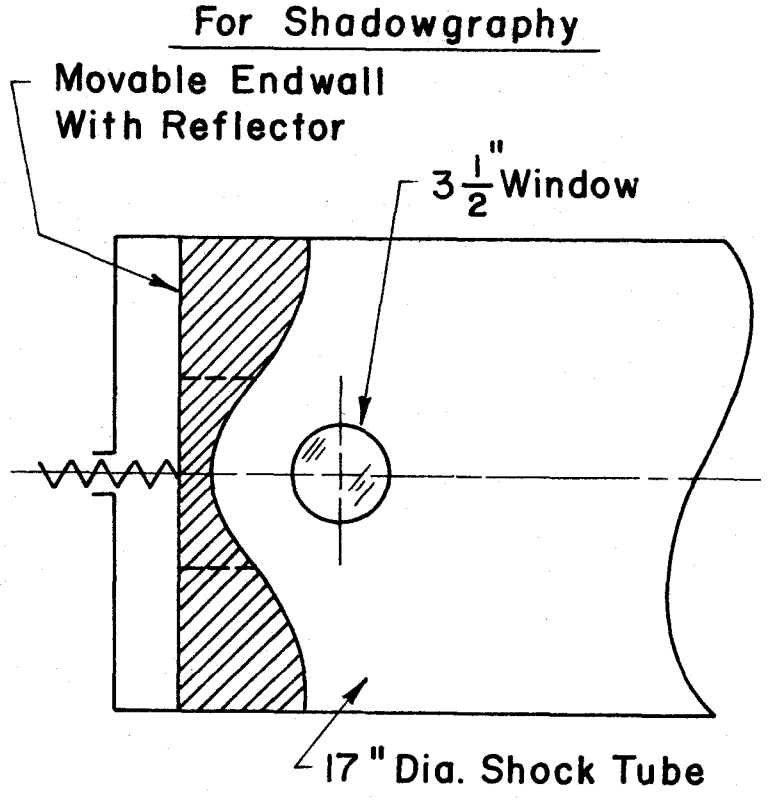

FIG. 10 MOVABLE ENDWALL

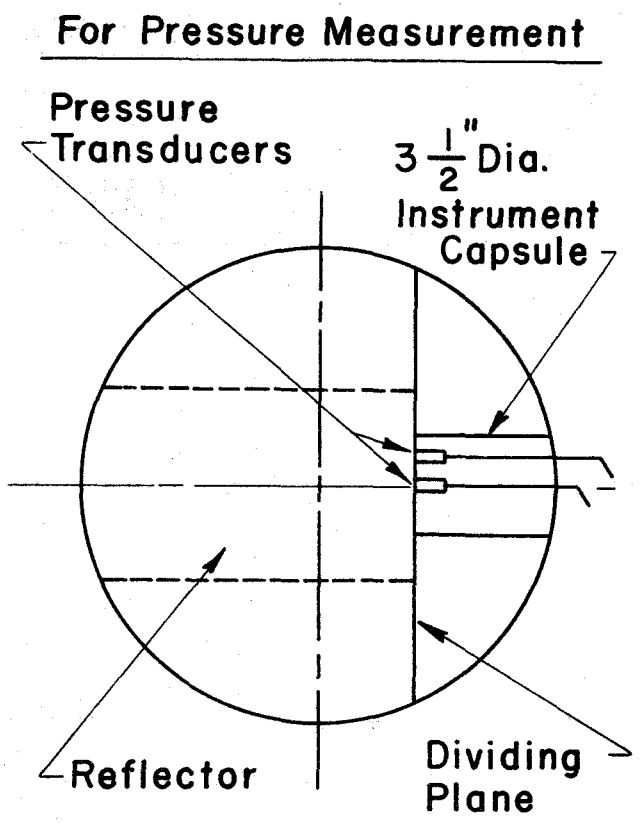

FIG. 11 VIEW FROM DIAPHRAGM

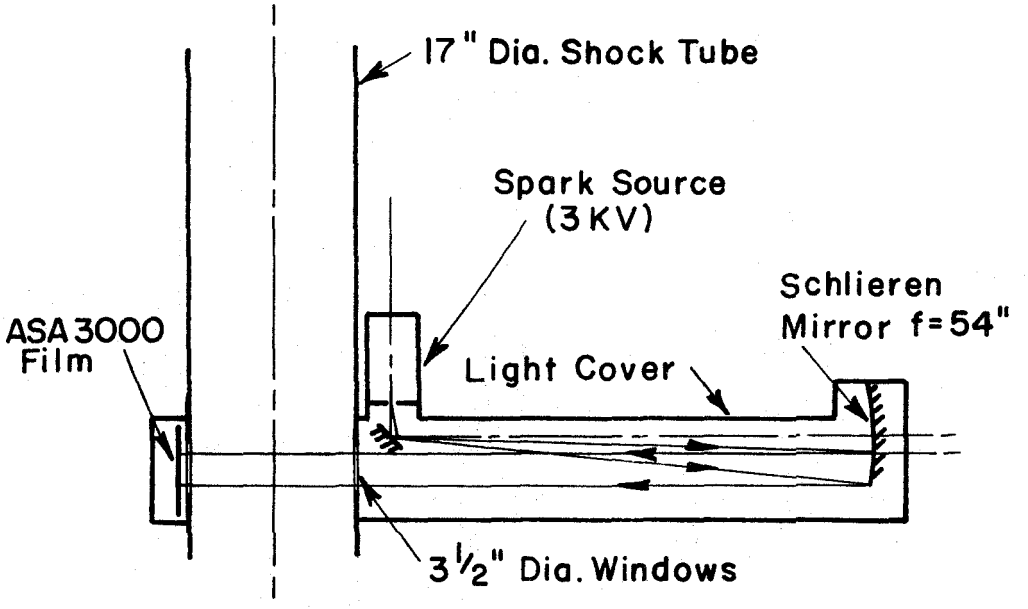

FIG. 12 SHADOWGRAPH SYSTEM

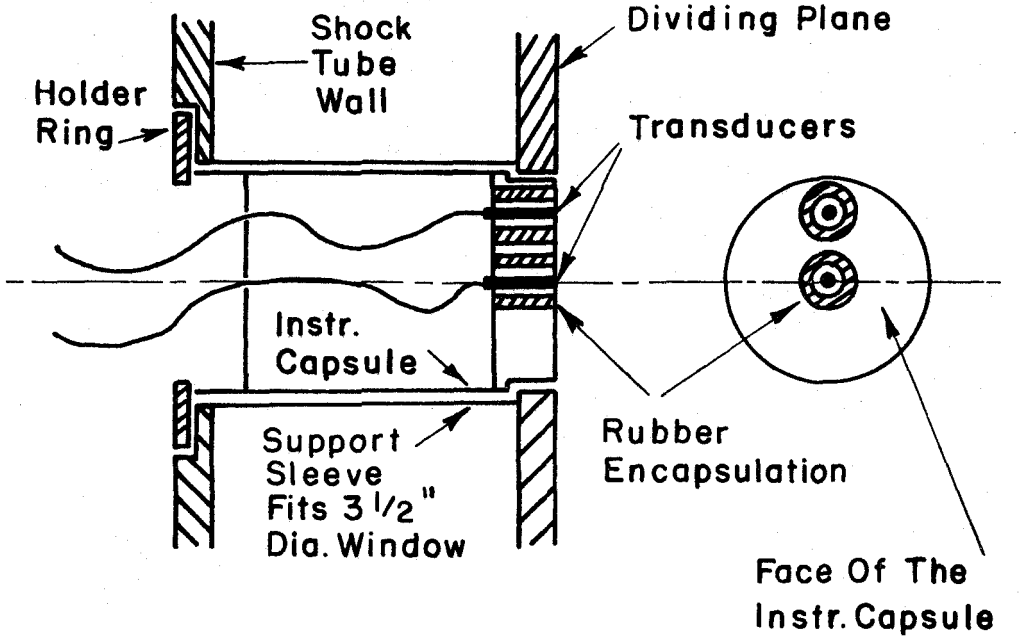

FIG. 13 DETAIL OF INSTRUMENT CAPSULE

used to make the light parallel. The aperture at the source had a diameter of .01", and this gave excellent resolution. Even hairline cracks in the silver of the mirror left an impression on the film, some 70" away. The 3 " windows in the shock tube were made of flat, optical glass and were mounted partly recessed and partly protruding into the shock tube, in order to minimize diffractions.

The spark was timed and triggered electronically. A piezoelectric gauge measured the incident shock wave and triggered a single sweep time base on an oscilloscope (Tektronix 555). A delayed trigger signal from the scope, with manually set delay, was amplified and used to trigger a thyratron vacuum tube. The thyratron in turn applied a 3000 V pulse across a small triggering spark gap. The ions provided by this spark across the main spark gap brought about the breakdown of the main spark gap and discharged a bank of capacitors. The time taken by the process, after the delayed trigger signal from the oscilloscope occurred, was of the order of a microsecond. (The original design for this spark gap was obtained from the University of Arizona.)

Thus a shadowgraph was obtained for each run of the shock tube, and by changing the delay setting on the oscilloscope it was possible to observe the flowfield at different stages of focussing.

2.4 Measurement of Transient Pressure Waveforms

After the different regions of flow were identified with spark shadowgraphs, transient pressures were measured at various points in the flowfield. High spatial resolution and a good high frequency response to transients like shock waves were necessary, and very small piezoelectric gauges were chosen for this purpose (PCB Piezotronics,

type 105A, risetime - 1 microsecond, sensitive surface smaller than 0.1" in diameter). The gauges have an integrated circuit amplifier coupled to the crystal, and show a very good sidewall response to a shock wave. However, when the gauge faces into the shock wave, ringing is observed. Also, mounting the gauge in midflow scatters the shock wave and the diffraction effects modify the signal considerably.

For two-dimensional flowfields, such as a line focus, these problems can be avoided by using a dividing plane. The dividing plane is parallel to the two dimensions of importance and has the pressure sensors mounted flush with the surface (Fig. 11). The influence of the boundary layer on the plane is seen to be rather minimal.

The dividing plane in the shock tube is shown in Fig. 11. It is supported in the shock tube through the instrument ports. The support is a hollow cylinder, and also serves as a housing into which the instrument capsule containing the pressure gauges can be introduced. Fig. 13 shows the instrument capsule mounted flush with the dividing plane. The capsule has two transducers, one in the plane of symmetry of the reflector, along the axis of the capsule, the other at a radius of 1" from the first. By rotating the capsule the second transducer may be placed at different distances from the plane of symmetry. The leading edge of the dividing plane was chamfered on the support side to minimize diffraction. Also the plane was sufficiently long, so the waves scattered by the support, etc., could not diffract around the leading edge into the flowfield during the time of measurement.

The dividing plane effectively modified the cross section of the shock tube. Portions of the movable endwall and the reflectors were

cut off so they fit this cross section. This made it necessary to finish all shadowgraphy before beginning the pressure measurement.

Proper mounting of the pressure transducers was found to be crucially important for good response. It was necessary to isolate them from the stress waves in the dividing plane. This was done by mounting the transducers in small brass mounts which were supported in a soft rubber cast (GE-RTV 118) as shown in Fig. 13. Also the mounting hole in the brass mounts had to be modified to cure pronounced ringing in the signal. The transducer has a small stub (0.1" dia. x 0.1" long) in which the crystal is mounted. It appears that anything touching this stub upsets the stress waves in the rod behind the crystal and leads to ringing. Some dimensions of the mounting hole and the seating ring had to be enlarged to prevent such contact and ringing, and some other dimensions had to be machined to a very close tolerance to ensure square seating.

Only preliminary pressure measurements were done in the axisymmetric flowfield created by a paraboloid reflector with a perfect point focus. Pressure histories were recorded at a few points on the axis of symmetry. At these points a piezoelectric gauge was located, facing the reflected waves. (PCB Piezotronics, 113 A 21, with a built in amplifier, risetime = 1 microsecond, sensitive surface smaller than 0.2" in diameter.) This was done with the help of an arm extending into the shock tube through an instrument port. The gauge showed no ringing when it faced into a shock wave, but considerable diffraction effects were seen due to its large size. The signal showed a spurious peak before it settled to the correct value. Also

the risetime increased considerably when the waves were incident at an angle. (These effects can be seen in the pressure measurements for a perfect point focus; sec. 3.7, Fig. 28.) However, it was possible to infer, qualitatively, the nature of the pressure variation.

All pressure measurements were recorded on oscillograms.

REFERENCES

Liepmann, H. W., Roshko, A., Coles, D. E. and Sturtevant, B. 1962 Rev. Sci. Instr. 33, 625.

III. PERFECT FOCI

This chapter deals with the experimental results and their interpretation regarding the behavior of shock waves near perfect foci. This is done in detail with one reflector producing a perfect line focus. First, the flowfield is observed with shadowgraphs for different incident shock strengths. Qualitative features of the reflected wave patterns are used to delineate various regions of the flowfield. Then, in correlation with these regions, some typical pressure waveforms are presented to indicate the changes occurring at and between the wavefronts. This is then summarized to show how the focussing is affected by the incident shock strength and how the focal processes control the maximum amplitude.

After this, the investigation is extended to different reflectors. Influence of the angle of convergence and the focal length is examined using reflecotrs with different angular apertures and focal lengths. The sharpness of the corners of a reflector is shown to have a minor effect on the focussing. The case of an axisymmetric point focus is examined to emphasize the generality of the observed phenomena. Finally, an approximate method for numerical simulation of some essential features of the focussing process is described. Results are presented for comparison with the observations.

3.1 Shadowgraphs and Wavefronts

For an incident shock of M = 1.1, Fig. 14 shows the reflection from a parabolic cylinder in various stages of focussing, at successive instants. (Reflector no. 1, Table 2). This behavior of the reflection

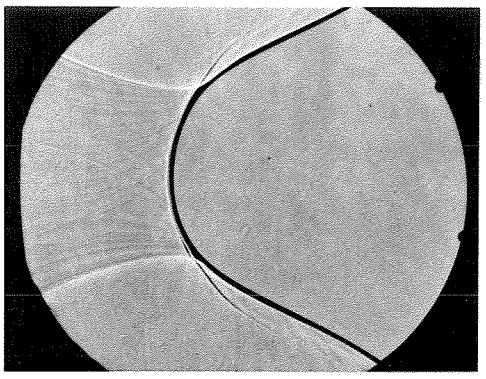

t = 0.0 ms

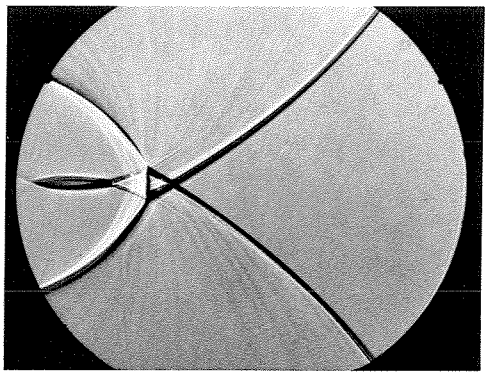

0.11

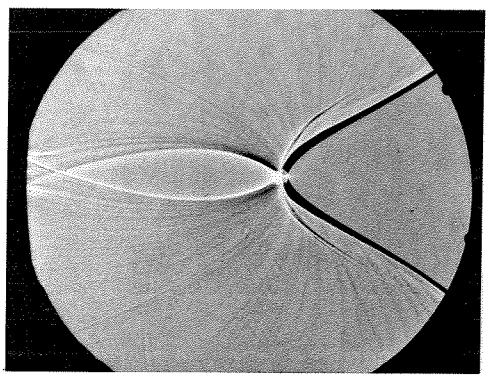

0.05

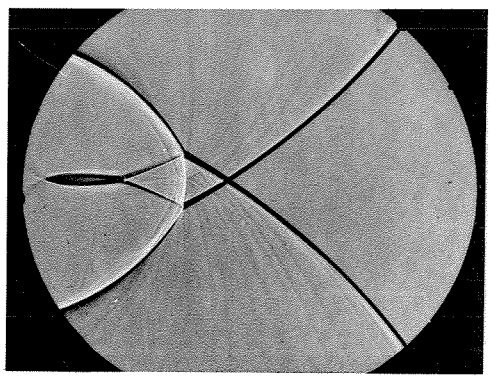

0.12

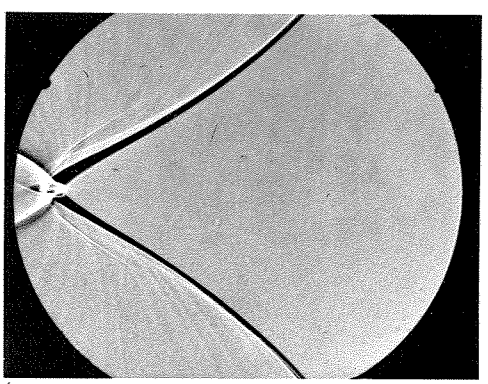

0.08

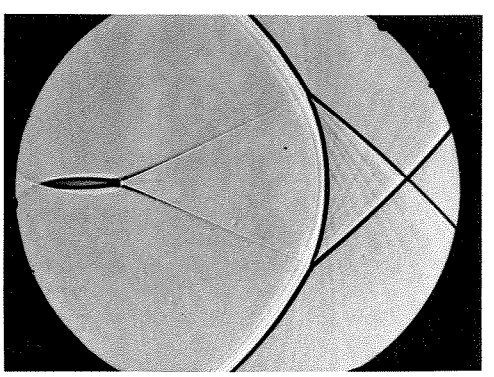

0.19

FIG. 14 SUCCESSIVE STAGES OF A WEAK SHOCK AT A PERFECT LINE FOCUS (M_s = 1.1, REFLECTOR I)

is typical of weak shocks, as may be inferred from the crossing and folding of the shockfront as it comes out of the focus. Nonetheless, nonlinear distortion effects are evident, especially near the focus. The dark lenticular region near the focus is the hot gas left behind by a strong shock.

In this sequence of shadowgraphs (Fig. 14), the reflection travels from left to right, and two different window locations are used. In the first two pictures, the reflector is immediately to the left of the frame. In the rest of the pictures, it has been moved back by 1 3/4".

In the first picture, the wavepattern has three different characters. The dark circular wavefront in the center, concave to the right, is the reflected shock traveling towards the focus. This wavefront has dark convex (to the right) extensions on either side, which are compressive diffraction fronts emanating from the sharp corners of the parabolid reflector. Behind these waves (on the left), are two circular light wavefronts, traveling towards the axis of symmetry. These are expansion waves, the counterpart of the compressive diffraction fronts from the corners of the reflector (cf. Fig. 7).

In the second picture the shockfront has converged towards the focus, and the diffracted expansions behind it have just passed through each other. In other words, the expansion from the lower corner of the reflector (convex upwards, traveling up) in the lower half of the first picture is now in the upper half of the second picture (still convex upwards, traveling up). The situation is symmetric for the other expansion. This picture exhibits an important nonlinear

effect. The intersections of the expansion waves with the shockfront have met each other, before the shockfront has reached the focus. In the linear picture, they arrive at the focus together with the shock-front (Fig. 7). Also, this picture shows an important feature of the diffraction wavefield behind the converging shockfront. Close to the shock, a dark region of compression waves can be seen developing ahead of the diffracted expansion fronts.

In the third picture the shock is at the focus, and in the rest of the sequence it is seen coming out of the focus with a crossed and folded configuration, leaving behind a region of hot gas at the focus. The compressive diffraction fronts from the corners of the reflector have crossed in front, and thus precede the focussed shock, which follows between the folds. The two tails of the "focal spot" are the slipstreams of the folds in the shock. The folds look very much like three-shock intersections, even when they are very close to the focus. This effect is due to the shocks attached to the folds on the outer side. These shocks appear to have formed from the compression fronts ahead of the diffracted expansions mentioned above. For such weak shocks, the tracks of the intersections in the fluid can be identified with shock-shocks. In fact, the focal hot spot seems to be enclosed by two shock-shocks, formed about the time of picture two. Thus the three-shock intersections develop from the intersections of the diffracted fronts with the shock. When these intersections turn around and cross again, they enclose the focal spot. From this point on, crossed and folded shockfronts are seen (cf. acoustic reflection, Fig. 8, also Fig. 7).

Fig. 15 shows the reflection of a shock of strength M = 1.3, in the same experimental configuration. This sequence of shadowgraphs shows the strong-shock behavior. Again, the intersections of the diffracted waves with the shock meet and turn into three-shock intersections before the shockfront gets to the focus. This occurs much earlier in this case. The stem shock of the intersections is surprisingly plane, and leaves the fluid in the focal spot with a higher entropy than its surroundings. In contrast to Fig. 14, the shock-shocks in this case do not turn around, but simply spread apart, and the focal spot never closes. Consequently, the configuration of waves obtained is not crossed and folded, but is flattened in some sense (cf. nonlinear reflection, Fig. 8). In the last two pictures, the waves have left the field of view, and only the slipstreams of the three-shock intersections are seen. The slipstreams are shear layers in addition to entropy layers and evidently become unstable. In fact, at the beginning of the focal spot the layers cross, and in the last picture, this crossing appears to be forming into a jet.

A selection of five such shadowgraph sequences for five different incident shock strengths is shown in Fig. 16. The sequences of Fig. 14 and 15 are respectively third and fifth from the top. The fourth sequence, M = 1.2, shows a borderline case between crossing and not crossing of the shockfront. In this case, the shock-shocks turn around and come very close to a second crossing, but then move away. The focal spot is almost pinched off at that point, but not quite, and the waves leaving the focus are not crossed. For shocks weaker than this the shock-shocks cross twice, giving a finite focal spot and

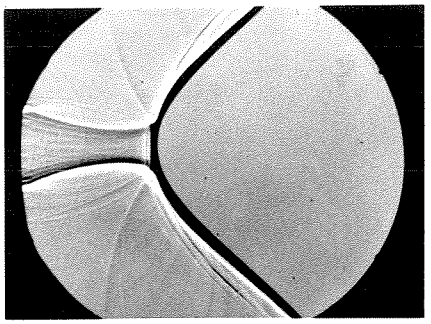

t = 0.0 ms

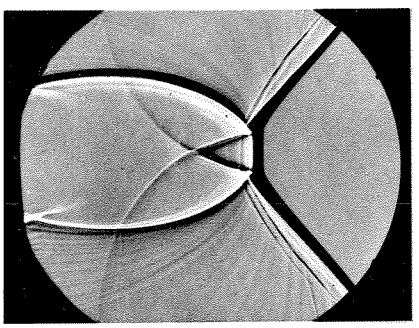

0.05

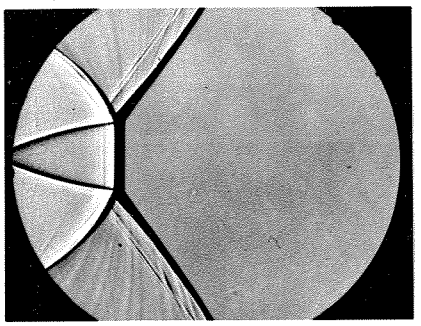

0.10

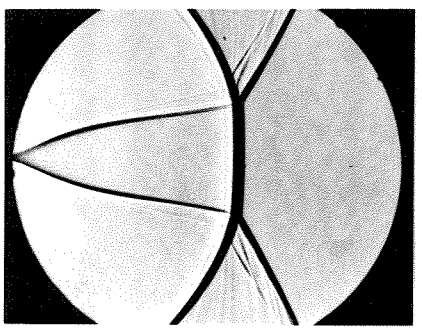

0.16

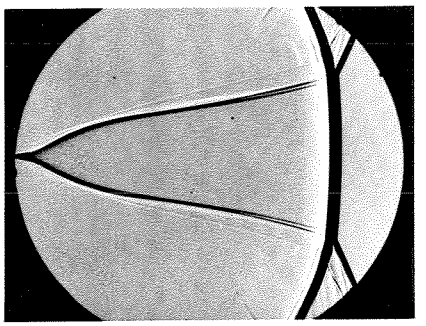

0.21

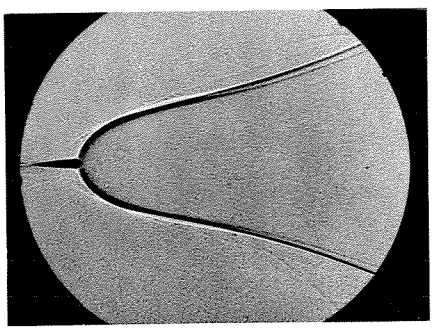

0.36

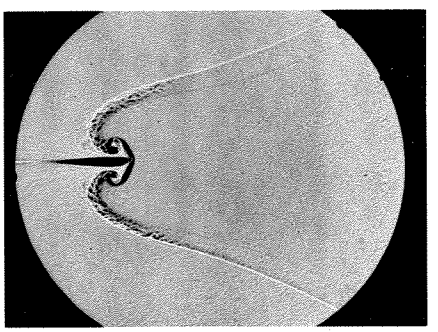

0.76

FIG. 15 SUCCESSIVE STAGES OF A STRONG SHOCK AT A PERFECT LINE FOCUS (M_s = 1.3, REFLECTOR 1)

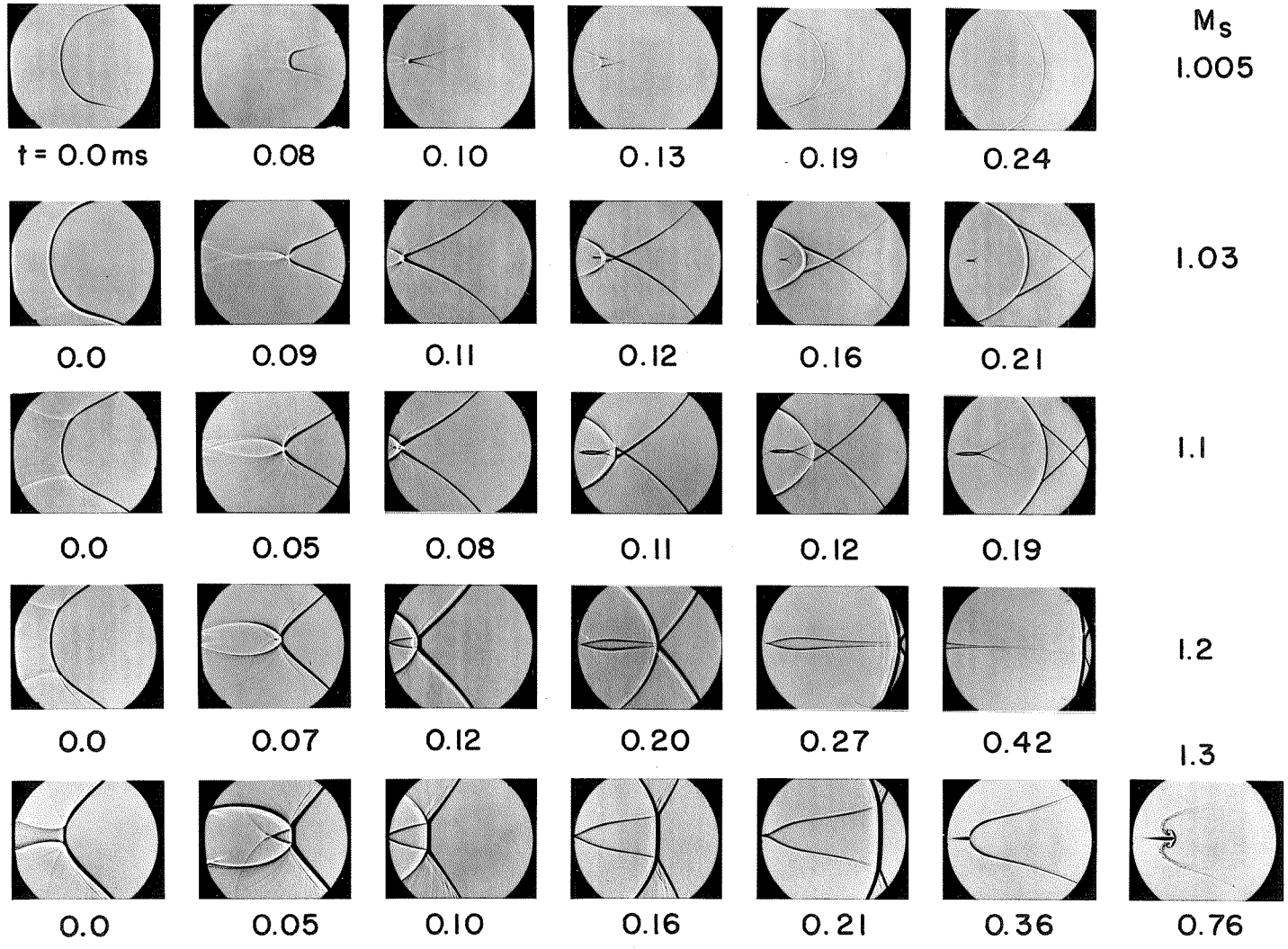

FIG. 16 EFFECT OF SHOCKSTRENGTH ON A PERFECT LINE FOCUS (REFLECTOR I)

crossed shockfronts. The stronger the shock, the larger the focal spot and the smaller the triangular loop in the shockfront. For shocks stronger than the transition shock strength (in this case, M = 1.2), the focal spot becomes semi-finite and the loop disappears.

In the focal spot, the shock is plane and normal, and the amplitude must be finite. Thus, nonlinearity spreads the focus and gives a finite maximum amplitude.

Figures 17, 18, 19 and 20 summarize the situation schematically into four processes, perfect focus of sound pulses, weak shocks, moderately strong shocks and strong shocks. The typical wavefront patterns for each are now shown together. The trajectories of the three-wave intersections (three-shock intersections or intersections of diffraction fronts with shocks) are shown with dotted lines for each case. In terms of shock dynamics, these are characteristics of waves on the shockfront, which turn into shock-shocks. Their further behavior determines the outcome of the process. If these curves cross a second time, enclosing the focal spot, crossed shockfronts occur. Otherwise, the focal spot extends to infinity, and the shockfront never crosses itself. In the limit of infinitesimal amplitude, these curves reduce to the rays (of geometrical acoustics) that confine the focussing shock, in Fig. 17.

3.2 Pressure Traces and Waveforms

The trajectories of the three-wave intersections divide the flowfield into different regions. These regions can also be identified with the kinds of waves occurring in them. This is shown in Fig. 21 with the help of pressure traces taken at different points in the various

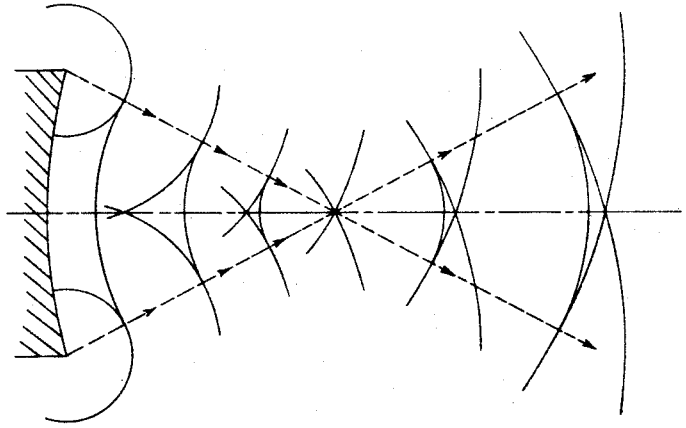

FIG. 17 SOUND PULSE AT A PERFECT FOCUS

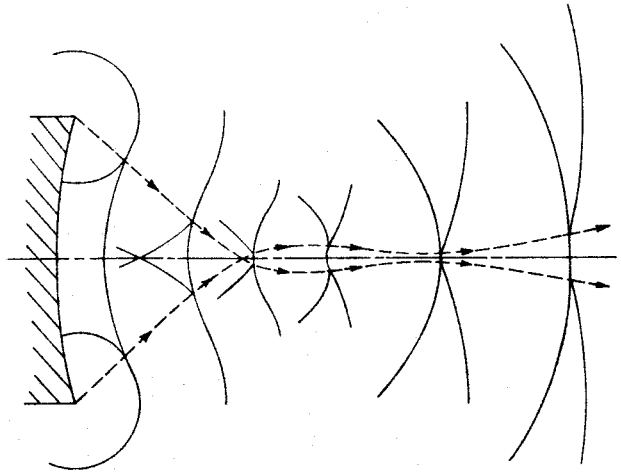

FIG. 19 MODERATELY STRONG SHOCK AT A PERFECT FOCUS

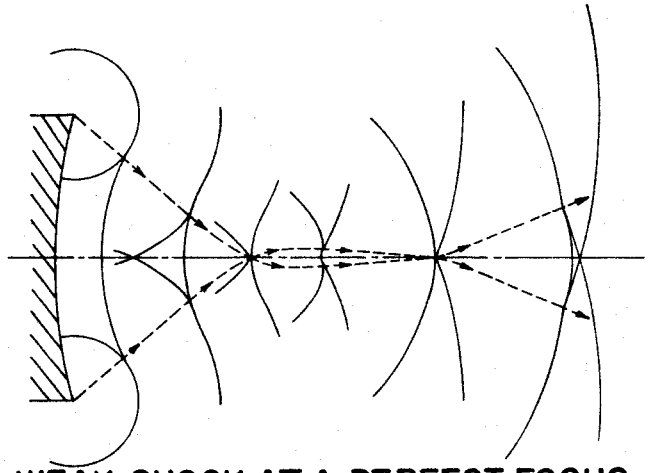

FIG. 18 WEAK SHOCK AT A PERFECT FOCUS

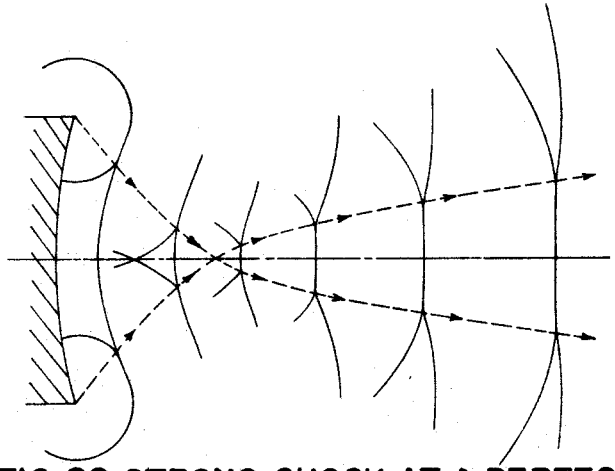

FIG. 20 STRONG SHOCK AT A PERFECT FOCUS

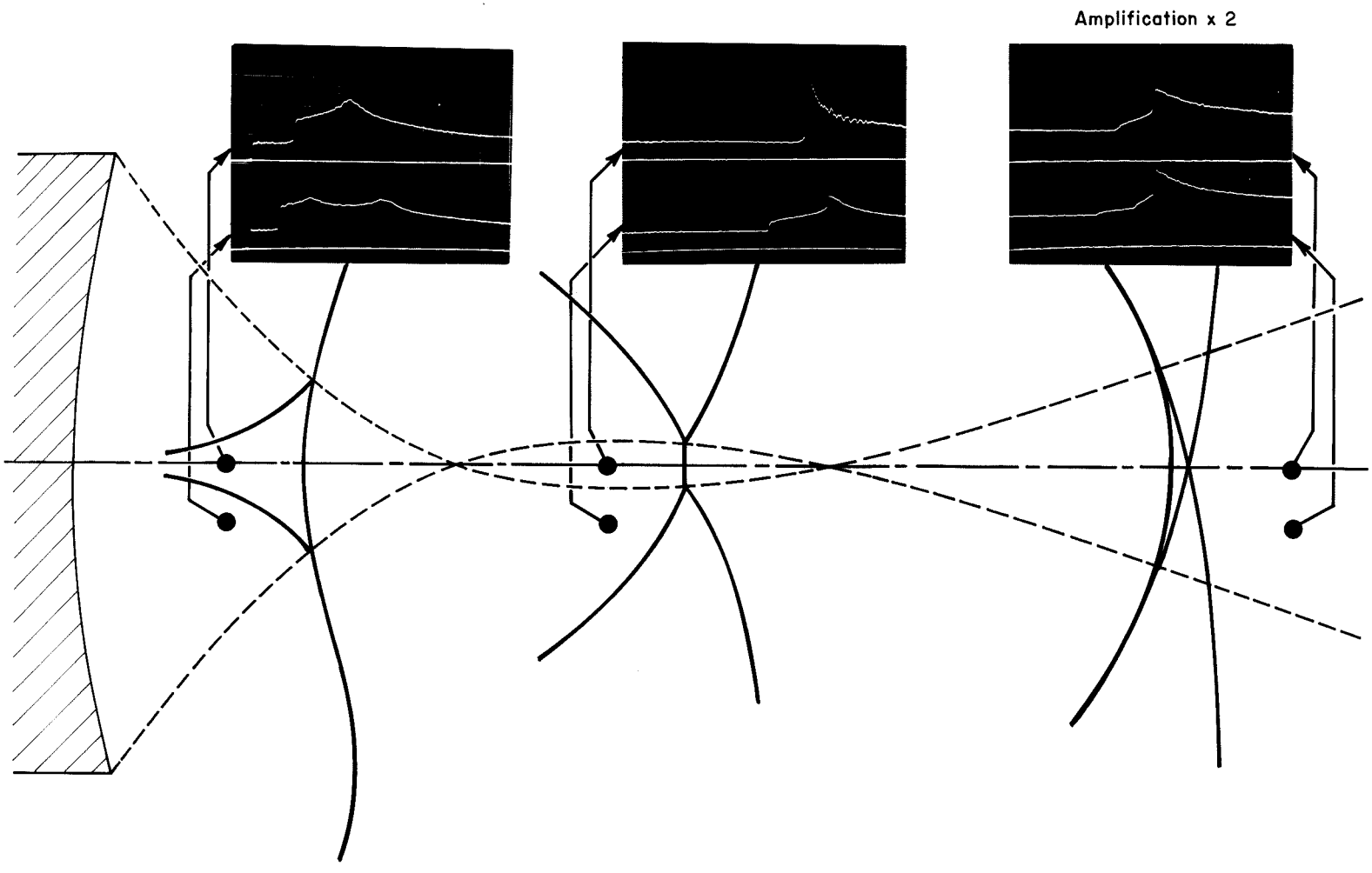

FIG. 21 PRESSURE TRACES FOR A PERFECT LINE FOCUS
(REFLECTOR I, M_S = 1.1, 5.9 psi/cm, 50 μ sec/cm)

regions. The different wave patterns (traveling to the right) before, at and after the focus are shown. The shock-shocks (dotted) cross twice and the final wave pattern is crossed, indicating this as the behavior of a weak shock. On the pressure traces, time increases to the right (abscissa), and pressure increases upwards (ordinate). Shocks are seen as discontinuities of pressure whereas diffracted expansions appear as discontinuities of slope. The different wavefronts can be correlated with the corresponding pressure variations. For points closest to the reflector, the first pressure jump on the traces corresponds to the incident shock.

A great deal of pressure variation can be seen between the wavefronts. Thus, the pressure rises smoothly behind the leading shockfront in all regions except the focal region. The pressure invariably drops after the last wavefront, in all regions. However, the feature of crucial importance is the sharp expansion following the strong stem shock in the focal region.

Even though only the weak shock case is shown, the pressure traces remain qualitatively the same in all cases. For strong shocks, the focal region extends to infinity, and the last region with the crossed shockfronts does not occur. Then the same pressure trace typical of a focal region (an expansion following the stem shock) is observed all along in the extended focal region, even far away from the focus.

The pressure field of each wave pattern can be visualized with the help of the waveforms. If the instantaneous value of pressure at each point is plotted normal to the plane of a wave pattern in Fig. 21, a pressure surface is obtained. Isometric views of such surfaces

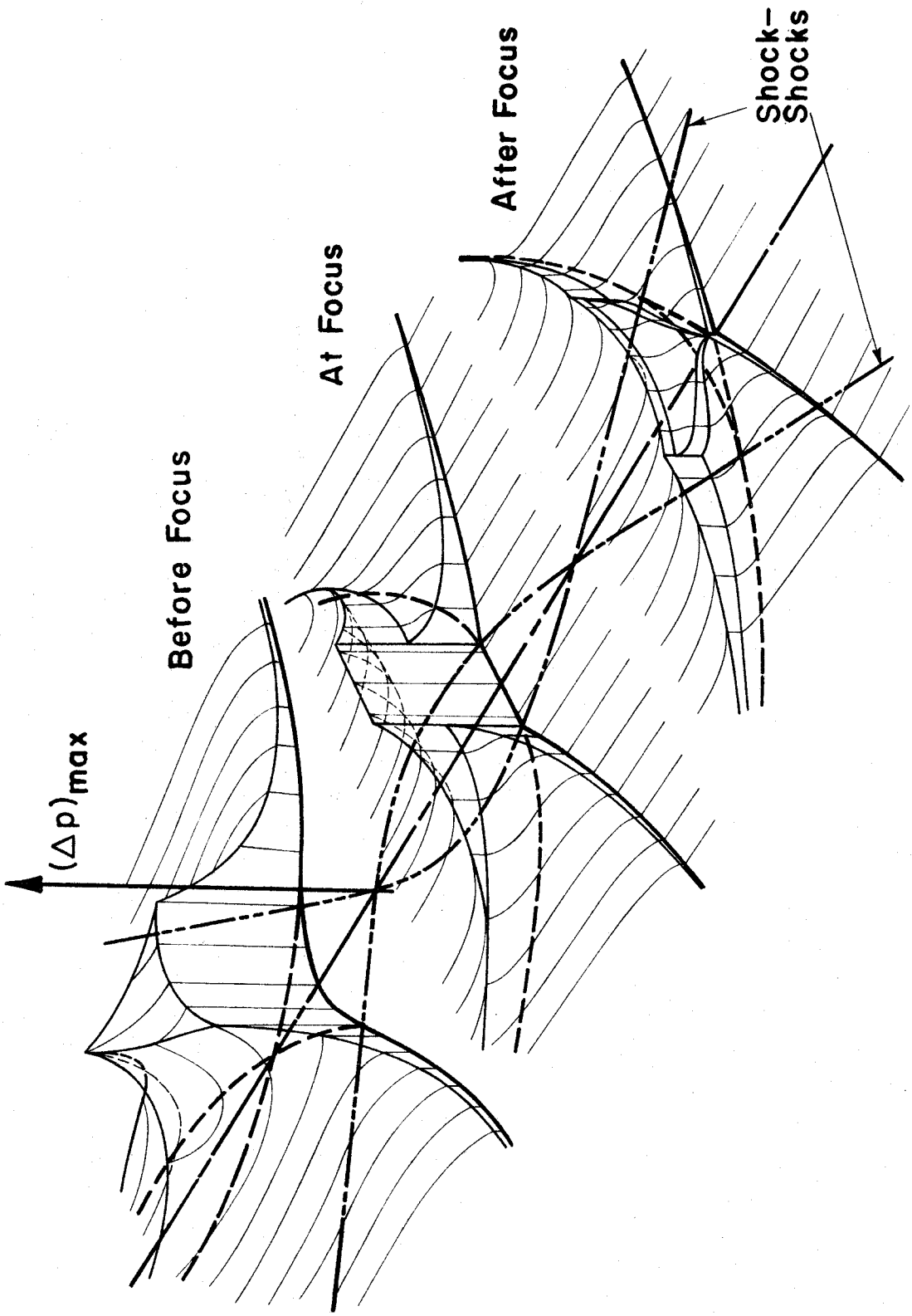

FIG. 22 PRESSURE FIELD NEAR A PERFECT LINE FOCUS

(only qualitative) corresponding to the three wave patterns are shown in Fig. 22. The wavefronts (heavy lines) are seen on the ground, traveling towards and to the right of the observer. The wavefronts and the shock-shocks correspond with those of Fig. 21. The pressure is shown vertically upward. Lines of intersection of the pressure surface with planes parallel to the plane of symmetry (light lines) indicate the wavelike nature of the surface. In fact, these intersection curves approximately represent the pressure trace observed in a corresponding location on the plane of wave patterns. This is seen if the observed pressure trace is held in a plane parallel to the plane of symmetry with pressure upward and time increasing in the direction opposite to the general direction of wave motion. The correspondence is not exact, because a wave pattern and its pressure surface are instantaneous, whereas the pressure trace is not. On the other hand, a pressure trace represents occurrences at a point in space, but not the wave pattern. However, in regions where all the waves are traveling roughly in the same direction, the correspondence is quite good. In regions where the waves travel in very different directions, this correspondence does not exist (for example, near the reflector).

These views of the pressure surface couple the pressure traces observed at various locations into an integrated picture of the focussing process. It is reasonably simple from here to obtain the pressure surfaces for intermediate times, for example, when the shock-shocks are crossing. The most important fact, however, is that the sharp expansion following the stem shock in the focal region arises from a combination of the two expansion waves traveling behind the shock.

These were shown to be due to diffraction at the corners of the reflector (Fig. 7). In fact, it is clear that the first crossing of the trajectories of three-wave intersections is the point of maximum amplitude; the amplitude is severely attenuated at any later instants by the two overtaking diffracted expansions. These expansions also carry a smooth compression ahead of them. Near the focal region parts of this compression form into shocks along the same diffraction front. Thus, nonlinear effects lead to the formation of the three-shock intersections. Later, when the waves cross, the shock coming out of the focus occurs on the same front and has the same character; a smooth compression followed by a shock and an expansion. Also, the nature of the diffraction fronts is seen clearly in regions away from the focus. The pressure rises (or falls, for an expansion) approximately as the square root of time (except for a small shock that leads the compressive fronts, which is clearly a nonlinear effect).

For weaker shocks, the focal region becomes smaller and the three-wave intersection trajectories tend to the rays of geometrical acoustics. The point of maximum amplitude shifts towards the focus. This implies larger maximum amplification for weaker shocks. In the limit of infinitesimal shock strength, the whole picture is acoustic and may be obtained from the behavior of sound pulses. It is interesting to note that the focussed shock, with a compression leading it and an expansion following it, turns into a logarithmic front in the acoustic limit (sec. 1.2b, Fig. 7).

Fig. 22, with its crossed shockfront, represents the focussing of a weak shock. For strong shocks, where the crossed and folded

waves do not occur, the focal region extends to infinity. The wave-forms observed in this extended focal region indicate that the pressure surface there is similar to that near the focus.

3.3 Peak and Maximum Amplitudes

The pressure surfaces show the local variations of pressure at different instants. The change in their amplitudes from instant to instant is represented by plotting peak amplitudes at various locations along the axis of symmetry (Fig. 23). The peak amplitude (maximum amplitude observed at a point) is normalized with the pressure jump across the normally reflected shock. The distance from the focus, along the axis, is normalized with the focal length.

The topmost curve in Fig. 23 shows the measured peak amplitudes at points along the axis. As can be seen from Fig. 22, the shock amplitude is smaller than the peak amplitude, outside the focal region. The variation of this shock amplitude, outside the focal region, is shown by the two lower curves. They seem surprisingly close to the $\sqrt{f/|x|}$ dependence of acoustic waves, in regions away from the focus (f = focal length = 2.375"). In the focal region, the shock amplitude becomes indistinguishable from the peak amplitude, as seen in Fig. 22. The apparent jump in the shock amplitude is connected with the simultaneous formation of the three-shock intersections at this point.

In the focal region, the shock amplitude (which is also the peak amplitude) diminishes as it travels along the axis. It is believed that this is due to the sharp expansion behind the stem shock overtaking it and reducing its amplitude. At the end of the focal region, the three-shock intersections pass through each other, and a focussed shock is

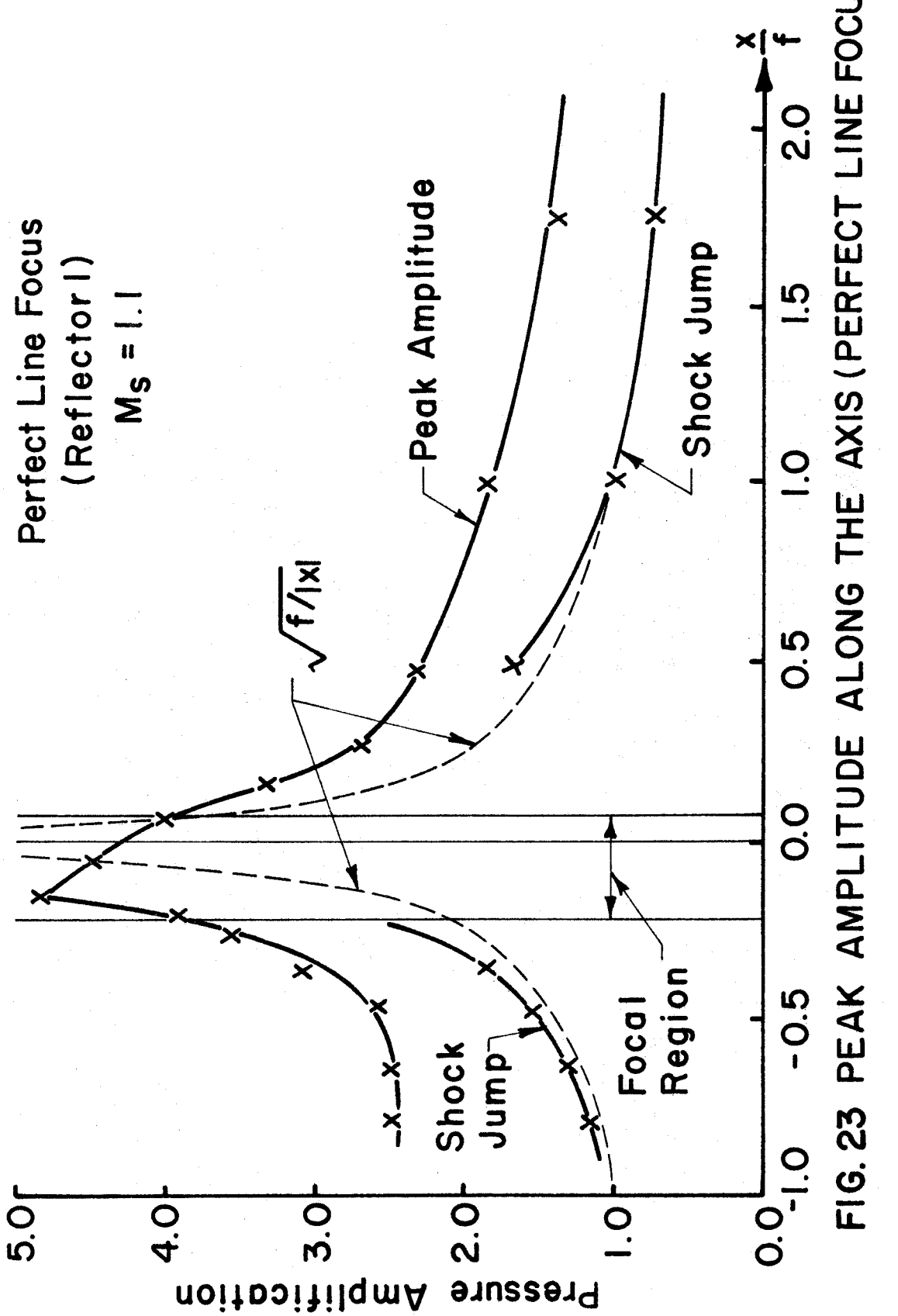

FIG. 23 PEAK AMPLITUDE ALONG THE AXIS (PERFECT LINE FOCUS)

formed (according to Fig. 22). Its amplitude at formation cannot be resolved with the present pressure sensor. However, the peak amplitude seems to drop more rapidly beyond this point, which marks the end of the focal region.

The amplitude at the beginning of the focal region is expected to be the maximum amplitude. However, the measurements do not indicate this. This is attributed to the limited resolution of the pressure sensor. It can be seen from Fig. 22, that the peak in the pressure surface is very sharp near this point (both along the axis and laterally). Further, the amplitude of this peak goes through a sharp maximum at this point. Therefore it is quite expected that the pressure sensor with its finite sensitive area reads an amplitude substantially lower than the maximum amplitude. (The size of the sensitive surface is about the same as the x symbols in Fig. 23.)

3.4 Influence of Shock Strength

This section re-examines the influence of incident shock strength on the focussing of shock waves. The two important features that best exhibit the behavior of focussing shock waves are the trajectories of the three-wave intersections and the distribution of peak amplitudes. The first of these is related to changes in the geometry of a focussing shockfront, whereas the latter indicates the change in maximum amplitudes.

Fig. 24 shows the trajectories of three-wave intersections starting from one corner of the reflector for different incident shock strengths. The situation is symmetric for the other corner, not shown here. The trajectories are traced directly from the

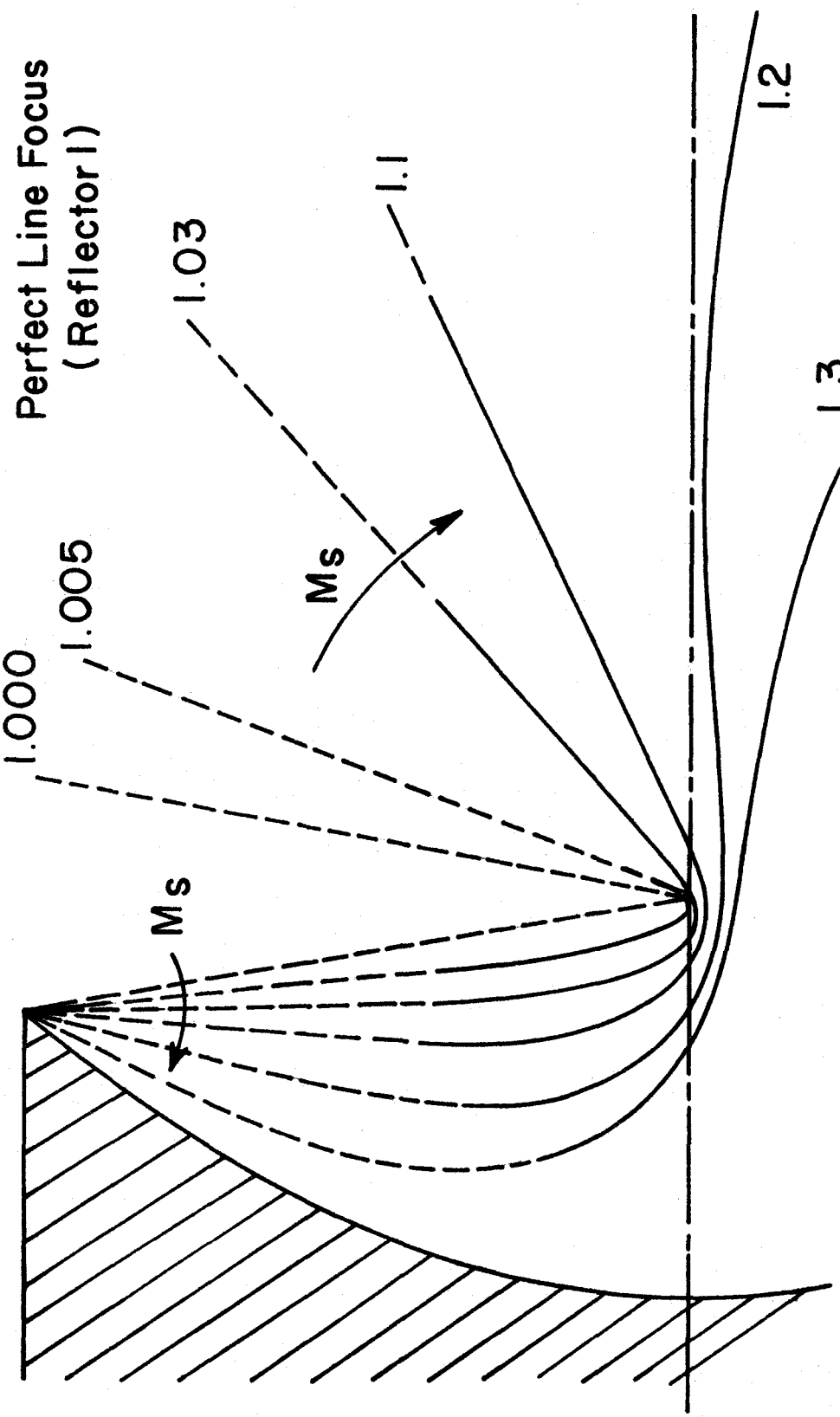

FIG. 24 EFFECT OF SHOCK STRENGTH ON TRAJECTORIES OF THREE-WAVE INTERSECTIONS (PERFECT LINE FOCUS)

shadowgraphs, such as in Fig. 16. The unobserved portions of the trajectories are shown dashed. For each trajectory, the region between the crossings with the axis of symmetry near the focus represents the focal region. For strong shocks only one crossing occurs, and the focal region is semi-infinite.

In the acoustic limit, the three-wave intersection occurs at the point of tangency between the shockfront and the diffracted expansion (see Fig. 17, for example), and its trajectory is the ray from the corner to the focus (shown dashed). For shocks of finite amplitudes, a three-wave intersection and its trajectory correspond, respectively, to a wave on the shock and its characteristic. These waves travel along the shockfront at speeds which increase with the shock strength. Thus the three-wave intersections of a stronger shock reach the axis much more rapidly. (This implies smaller maximum amplification for stronger shocks.) Near the axis, they turn into three-shock intersections and travel along shock-shocks.

After the focus, the three-shock intersections for the weak shocks travel into the axis of symmetry, like transient "inverted intersections", and are replaced by regular reflection at the axis (see sec. 1.3). This gives crossed wavefronts. On the other hand, for strong shocks, the three-shock intersections travel away from the axis of symmetry, like "direct intersections" of a Mach reflection. Consequently, the shockfront has no loop. This behavior of focussing shock waves seems consistent with the behavior shown in Figs. 8 and 9, and discussed in section 1.3.

The influence of incident shock strength on peak amplitudes is

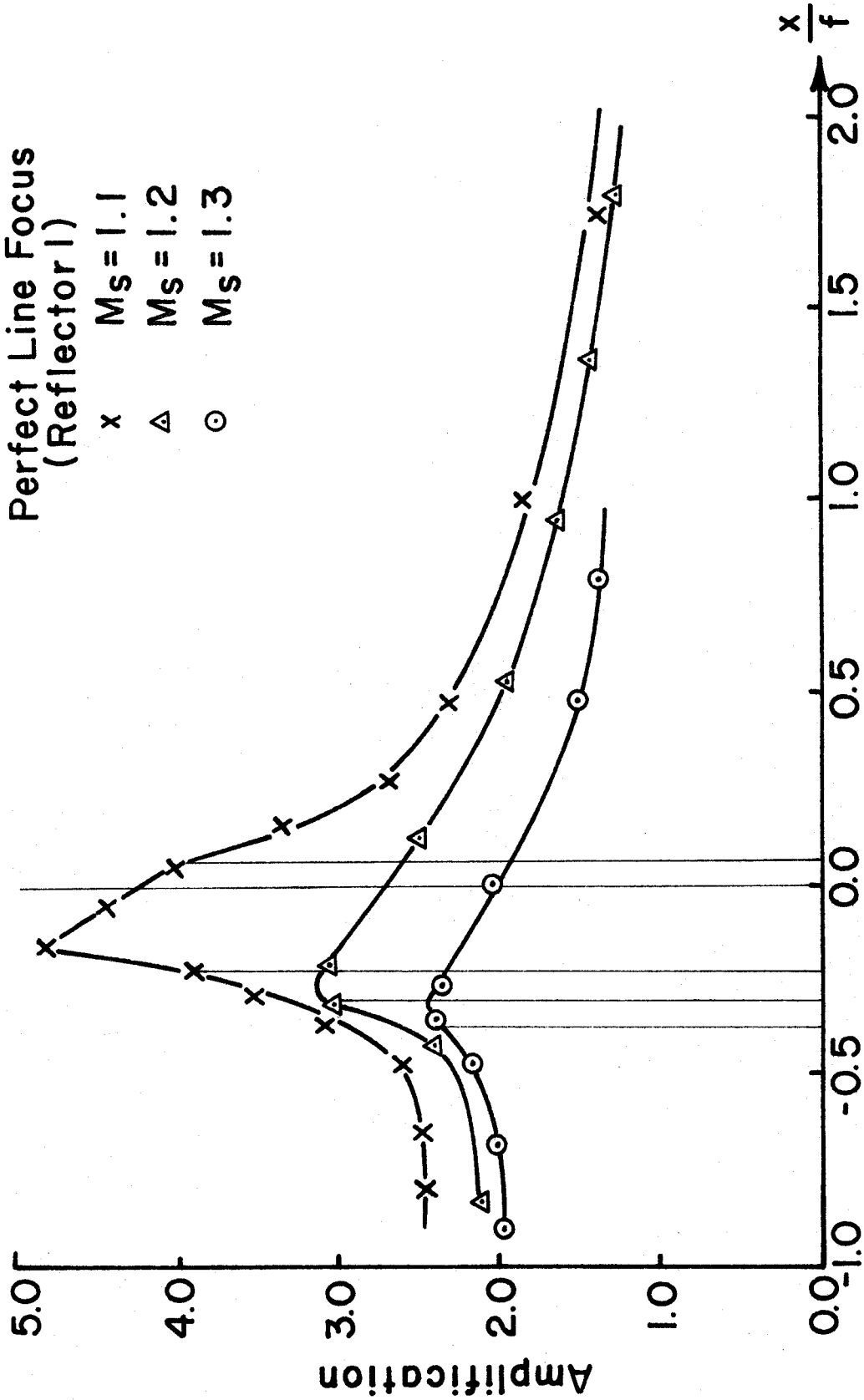

FIG. 25 EFFECT OF SHOCK STRENGTH ON PEAK AMPLITUDES (PERFECT LINE FOCUS)

shown by Fig. 25. Only the measurements for M = 1.1 and above are presented. For weaker shocks, the foci are very small and cannot be adequately resolved by the pressure sensor. The curve for M = 1.1 appears to have a discontinuous slope at the point where the focal region ends. For both M = 1.2 and 1.3, the focal region is semi-infinite, and such kinks do not appear in the peak-amplitude distribution. However, in either case, it seems certain that the diffracted expansions overtake the shock on the centerline, before it gets to the focus and reduce its amplitude. For stronger shocks, it is seen that the expansion waves overtake the shock earlier, with the result that the maximum amplitude is smaller.

Thus, the three-wave intersection trajectories show that the mechanism for the expansions to overtake the shock is basically non-linear. Further, the peak amplitudes indicate that the expansion waves reduce the amplitudes in the focal region by a nonlinear interaction. Therefore, in a given shock-focussing situation, the maximum amplitude is determined by the nonlinear behavior of finite amplitude waves.

3.5 Influence of the Angle of Convergence and Focal Length

Reflections from two other parabolic cylinders with shallower geometries have been examined. This implies smaller angles of convergence (angular aperture) of the reflected wave. The flowfield was observed only with shadowgraphs.

Even though the shockfronts are shallower in these cases, they undergo exactly the same processes seen in Fig. 16, which can be summarized by Figs. 17, 18, 19 and 20. However, the shock strengths

for which each case is observed are smaller. For example, the transition in the geometry of the shockfront from crossed to uncrossed waves occurs for relatively weak shocks. (Table 3 shows the range of shock strengths in which the transition occurs for each reflector.) It is also possible to examine the influence of change in the angle of convergence for a given shock strength. This is done in Fig. 26, using observed trajectories of three-wave intersections. (These trajectories are traced directly from the corresponding shadowgraphs.) It can be seen that for a smaller angle of convergence the focal region is larger. When the length of the focal region becomes comparable to the focal length, the transition to uncrossed waves occurs.

Physically, converging of the fronts and nonlinear acceleration of the shock in the center are competing effects. The waves cross if they are coming into the axis very steeply. On the other hand, if the stem shock in the focal region is strong or the convergence is slow, the shock accelerates out of the convergence, giving uncrossed waves. Thus, a rapid convergence suppresses nonlinear effects, whereas a slow convergence makes the focussing effectively more nonlinear.

It has been shown so far that the focussing of shock waves and its dependence on shock strength and convergence are basically due to the nonlinear distortion of the wavefield. It is well known that this distortion scales with time elapsed or distance traveled (see sec. 1.3). Therefore, the focal length or the radius of curvature is the natural length scale for nonlinear effects observed near a focus. For this reason, in Fig. 26, the trajectories of the shallower reflectors are scaled so the focal lengths of the three reflectors coincide. Thus,

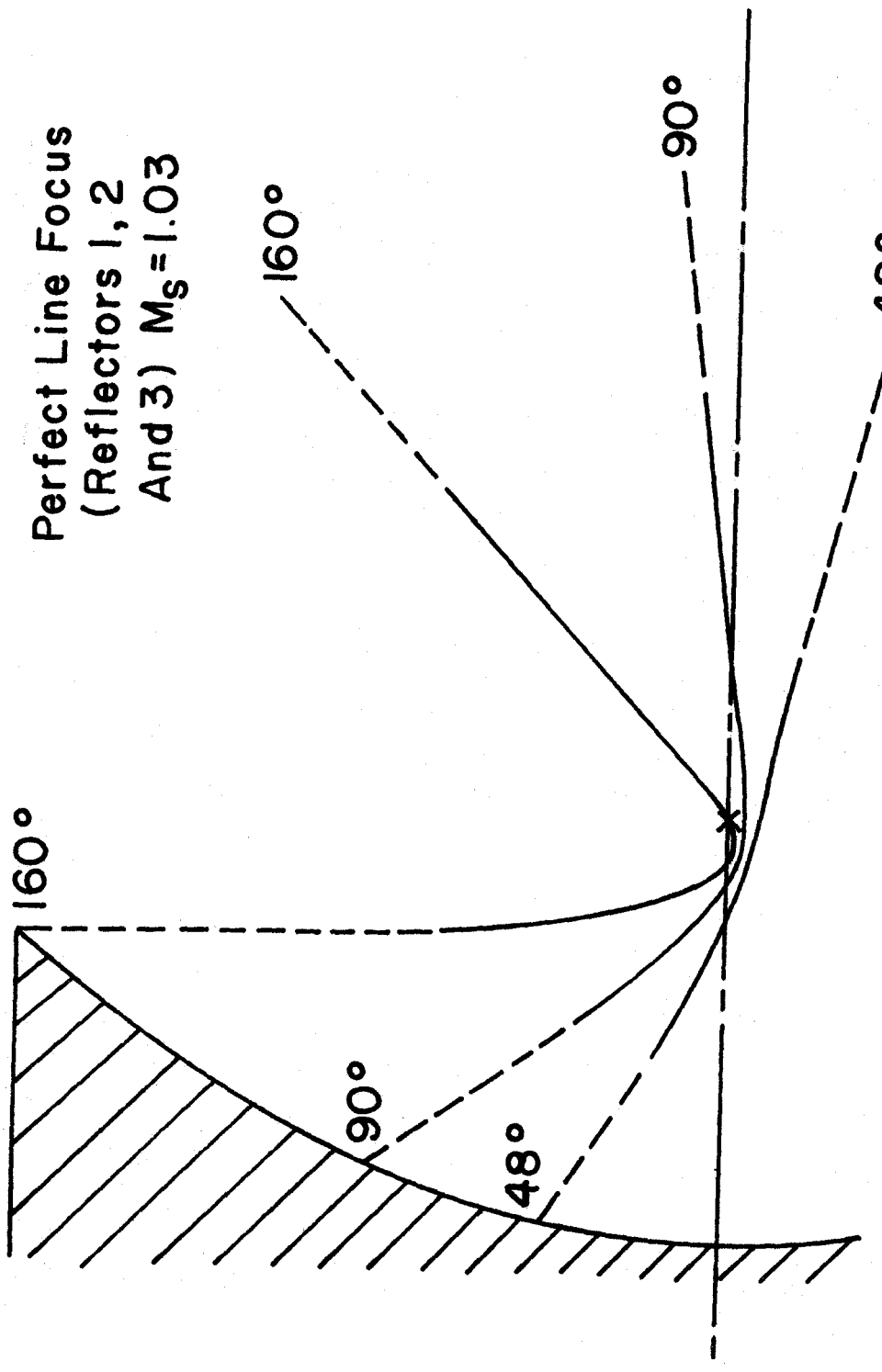

FIG. 26 EFFECT OF ANGLE OF CONVERGENCE ON TRAJECTORIES OF THREE-WAVE INTERSECTIONS (PERFECT LINE FOCUS)

when scaled with the focal length, the nonlinear phenomena in the focussing of a shock wave essentially depend only on the convergence and the shock strength.

3.6 Influence of the Sharpness of the Reflector Corners

For this purpose the reflector producing a perfect line focus was used (Reflector 1, Table 2). This was fitted into a flat baffle, so the incident shock reflected normally beyond the ends of the parabola. At the end of the parabola, the slope changed discontinuously to that of the baffle. Also, a rounded baffle that avoided this discontinuity of slope was tried. In this case, however, the radius of curvature was still discontinuous at the point.

These changes made very little difference to the wavefronts and the shock-shocks. Fig. 27 shows the late stages of reflections of weak shocks (M = 1.1) for the three configurations: reflector without a baffle (sharp corners), reflector in a flat baffle, and reflector in a rounded baffle. The close similarity suggests that the discontinuity in the curvature of the reflection leads to diffraction waves which are equivalent, as far as the focus is concerned.

This is not unexpected. The diffraction front depends on the discontinuity in the amplitude of the shock, which is approximately the same in the three cases. The final equilibrium pressure, far behind the diffraction fronts, may differ. However, the portion of the diffraction that is important near the focus is the leading edge of the expansion. Since this does not change very much, the sharpness of the corners of the reflector has only a minor influence on the focussing of a shock wave.

With Sharp Corners

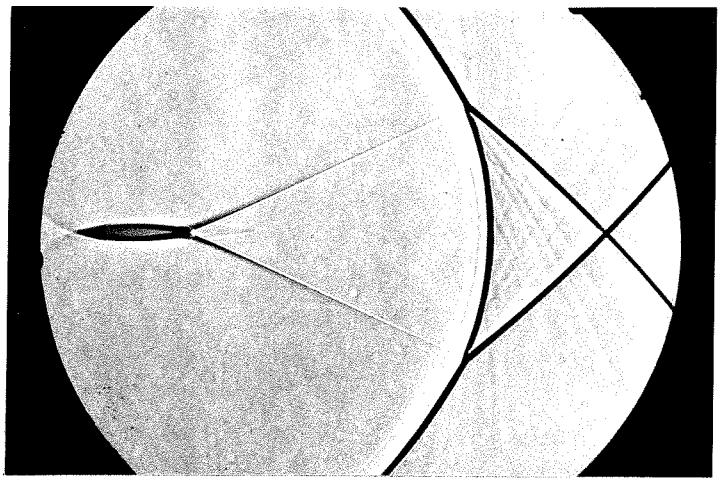

With A Flat Baffle

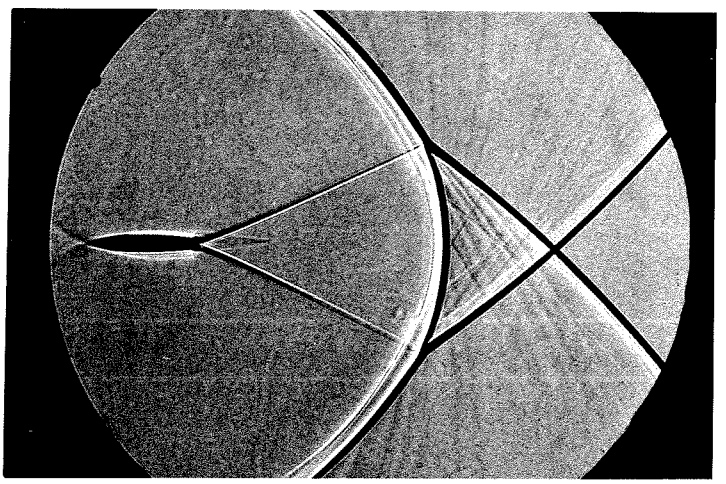

With A Rounded Baffle

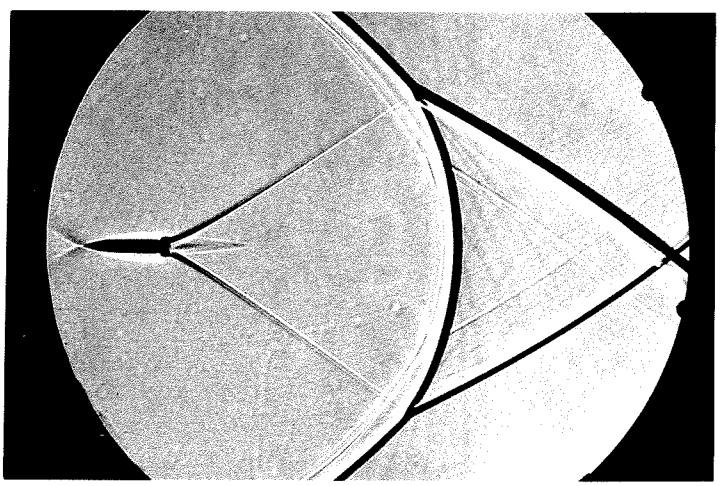

FIG. 27 EFFECT OF THE SHARPNESS OF REFLECTOR CORNERS (M_s = 1.1, REFLECTOR I)

3.7 Perfect Point Focus

This kind of a focus differs from the perfect line focus due to its axial symmetry. In this case, according to geometrical acoustics, not only does the shock go through a point focus, but even the diffraction wavefronts focus on the axis as they cross it. The sharp edge of the paraboloid reflector is a circle and the diffraction front emanating from it is a growing torus; all rays emanating from the circumference with a fixed inclination to the axis converge at a point on the axis, and different points on the axis represent foci for rays with different inclinations to the axis. Nevertheless, if projected onto a plane containing the axis, the wavefronts are identical to those of a perfect line focus (Fig. 7). The parallel beam shadowgraph automatically takes such a projection. However, its sensitivity is drastically reduced because, now, only the small portions of the shockfront tangential to the beam make a shadow.

Qualitatively, the shockfronts near a point focus look very much the same as in Fig. 16, and show identical changes with shock strength. Therefore, shadowgraphs from experiments on point foci have not been presented. Just as in the case of a perfect line focus, the behavior of the reflection in this case also can be separated into four cases: focussing of sound pulses, weak shocks, moderately strong shocks, and strong shocks (shown in Figs. 17, 18, 19 and 20). The critical shock strength for the transition in the geometry of the shockfronts is different in this case, due to the axial focussing of the diffracted waves.

The major effect of axisymmetric focussing is seen in the pressure waveforms, especially on the axis. Fig. 28 shows some

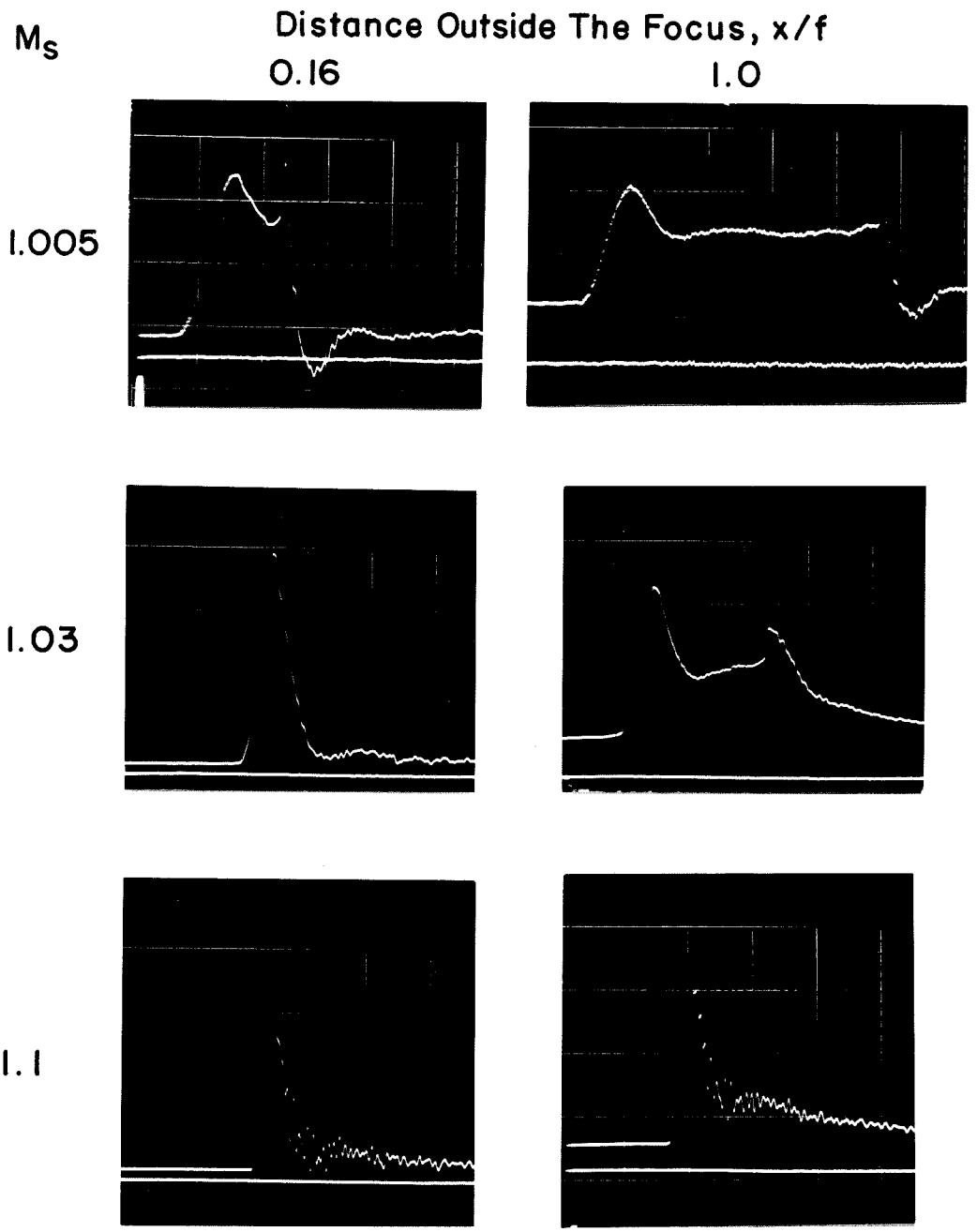

FIG. 28 PRESSURE TRACES AFTER A PERFECT POINT FOCUS (REFLECTOR 4, SWEEP - 20μ sec/cm)

pressure traces made on the axis outside the focus. The experimental configuration and the transducer are different in this case, as described in sec. 2.4. If the effects of finite size of the pressure gauge (sec. 2.4) are taken into account, the pressure traces of Fig. 28 can be qualitatively interpreted. In fact, the influence of nonlinearity can be shown quite clearly. For the traces in the top row and in the second row, second column, the diffraction waves arrive before the focussed shock. The focussed shock is inverted and follows the diffraction waves (sec. 1.2b, Fig. 7). Thus, the waveform has the appearance of a square pulse, consistent with the predictions of acoustics. The inverted "shock", however, seems to be preceded by a smaller shock not predicted by acoustics. The width of the square pulse is proportional to the size of the loop in the folded shockfront. Since the size of the loop increases with distance from the focus and decreases with increasing shock strength, the pulse width follows the same trends. In fact, in the bottom row, the pulse width is zero. This indicates that the probe is in the extended focal region; it is sensing the stem shock and the expansion wave behind it. This is consistent with the flattened shockfront shown by the corresponding shadowgraphs. The transition in the geometry of the shockfront occurs for an incident shock strength between $M = 1.03$ and $M = 1.1$, for this reflector.

3.8 Approximate Numerical Simulation

Trajectories of three-wave intersections describe a significant part of the behavior of focussing shock waves. Therefore, such trajectories have been computed based on a simplified geometrical

model for the motion of a three-wave intersection. Basically, the motion of the intersection of two fronts (or curves) moving with different velocities is found numerically. The difference in the velocities of the two fronts is assumed to be proportional to the shock strength (Appendix A). Then the trajectories can be calculated, provided the shape and strength of the shockfront are known a priori. Such information cannot be predicted by simple means in regions where the shockfront is strongly affected by nonuniform diffraction fields. In these regions, approximate forms of the observed shock shapes and the expected shock strength distributions are used (Appendix A).

Figs. 29 and 30 show the results of such computations. Qualitatively, the behavior of the computed trajectories is very similar to that observed in Figs. 24 and 26, respectively. (Crosses in Fig. 29 correspond to points on the trajectory for $M_s = 1.2$ in Fig. 24). In fact, even the critical shock strengths for the geometrical transition of the shockfront agree with the measured values (Table 3). With due consideration to the approximations involved, the good agreement with observations indicates that the basic mechanism behind this behavior of three-wave intersections is the inherent nonlinearity of shock waves. However, the method used here is very approximate and restricted, and and may not apply to other situations. A much more general and complete approach is that of shock dynamics, which represents the same aspects of the nonlinearity of shock waves in terms of waves on the shock, their characteristics and shock-shocks (sec. 1.3).

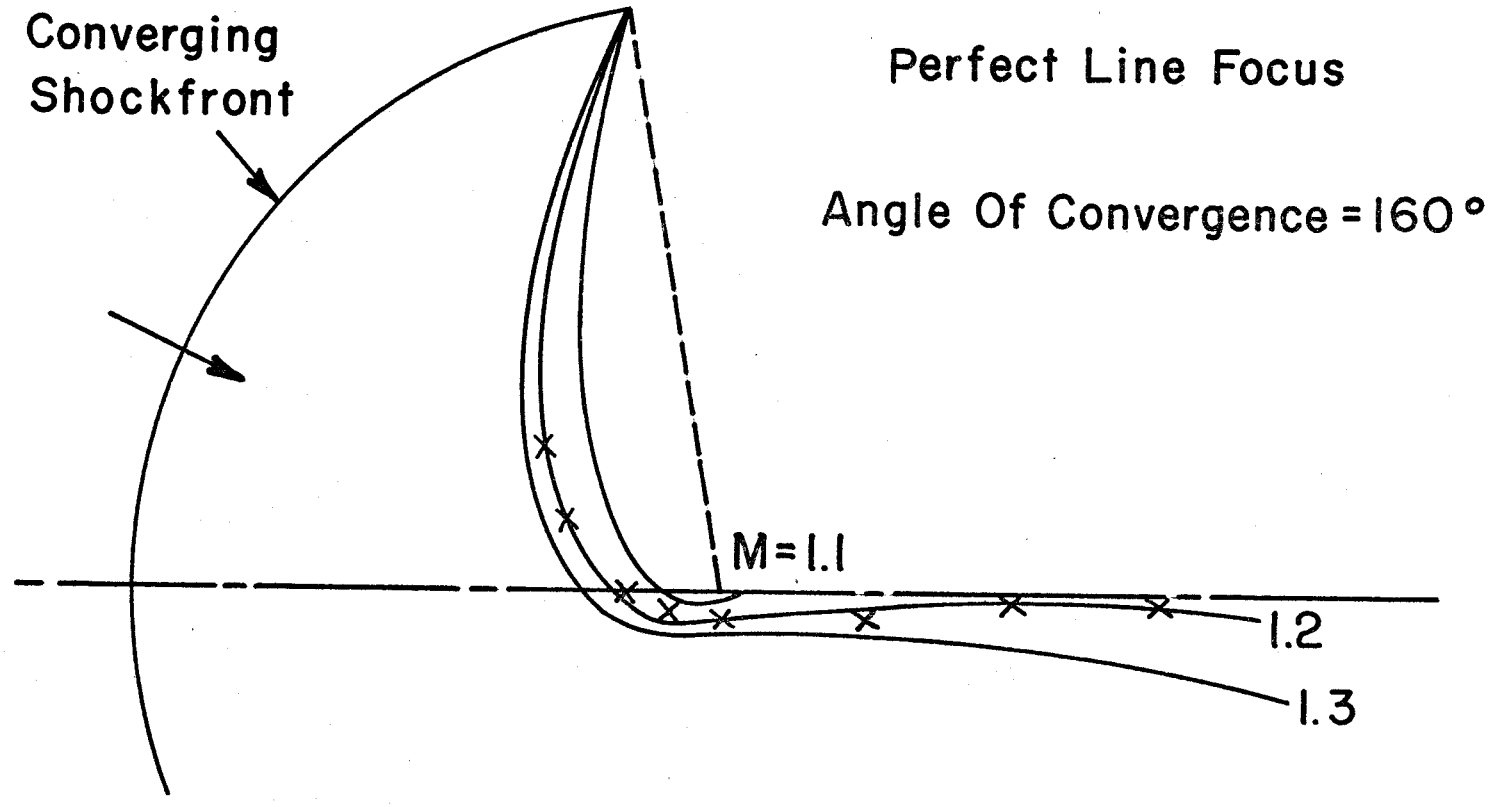

FIG. 29 COMPUTED TRAJECTORIES OF THREE-WAVE INTERSECTIONS, EFFECT OF SHOCK STRENGTH

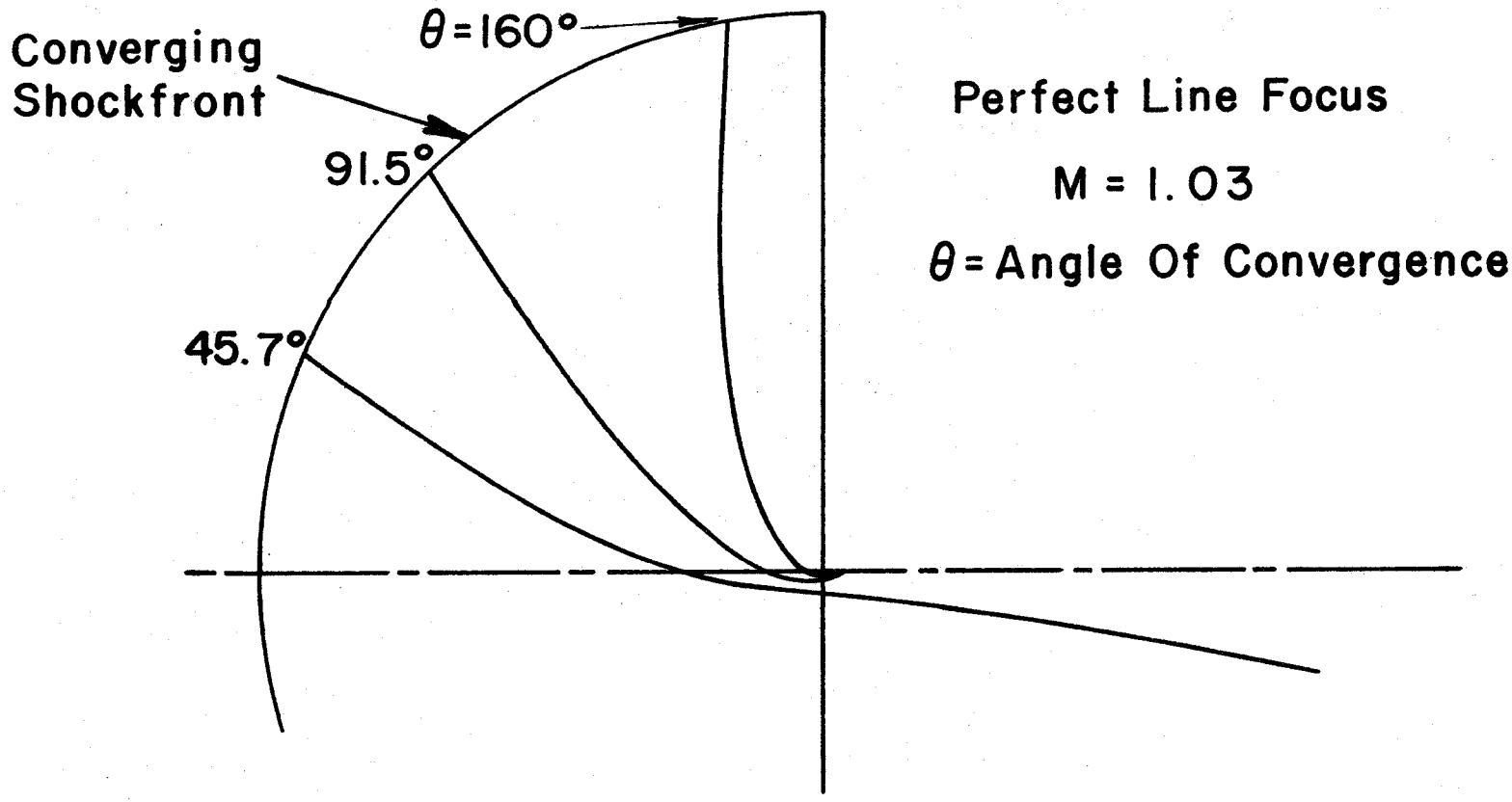

FIG. 30 COMPUTED TRAJECTORIES OF THREE - WAVE INTERSECTIONS, EFFECT OF ANGLE OF CONVERGENCE

IV. CAUSTICS, CUSPED AND SMOOTH

In this chapter, the behavior of focussing shock waves is investigated near an arete (a cusped caustic) and a smooth caustic. The approach is similar to that used in the case of perfect foci. An arete is examined in detail with shadowgraphs and pressure waveforms to identify the processes occurring near the cusp and near the rest of the caustic. Then the influence of shock strength is emphasized to show how the nonlinearity in the process is effective in controlling the maximum amplitude in the foci. All through, the features that are parallel to the perfect foci are pointed out and the important differences are described in detail. Finally, the case of a smooth caustic is examined in relation to the phenomena observed near an arete.

4.1 Shadowgraphs and Wavefronts Near an Arete

Fig. 31 shows four successive stages of a focussing shockfront near an arete. ($M = 1.2$ for the incident shock, the reflected front is traveling to the right.) This sequence represents the arete of a weak shock, as signified by the crossed wavefront configuration in the last picture (bottom row, on right). Nonetheless, occurrence of strong shocks near the focus is evident from the heated fluid (dark, peninsular region in the center).

The first picture of the sequence shows the reflected shock approaching the cusp of the caustic (dark curve, concave to the right). Near the most concave portion of the shockfront, some evidence of diffraction can be seen. This is quite expected, since the most concave portion is also the most amplified portion, being nearest to a focus.

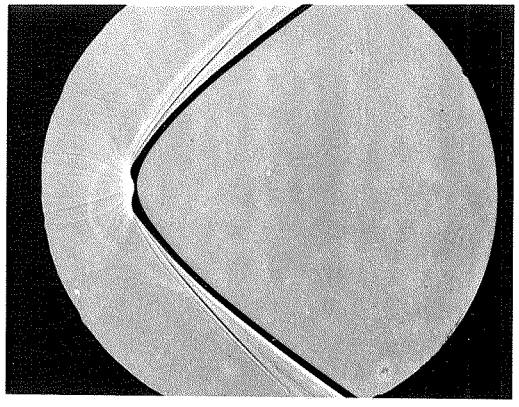

t = 0.0 ms

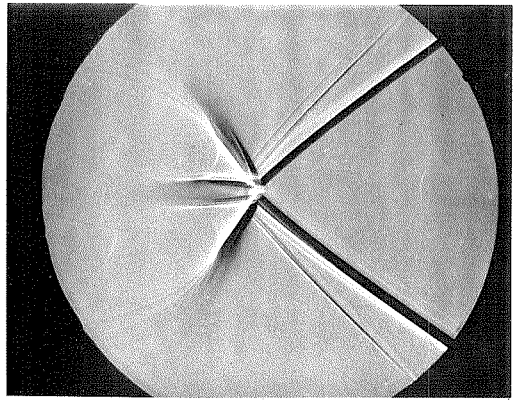

0.06

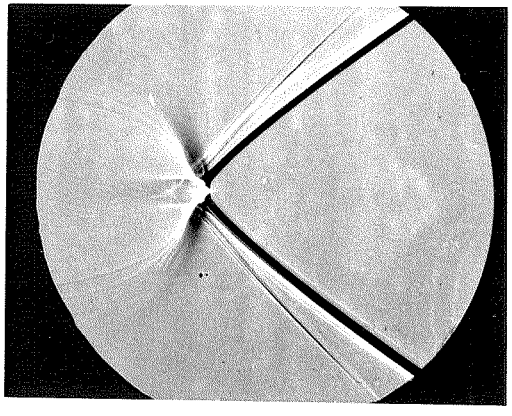

0.03

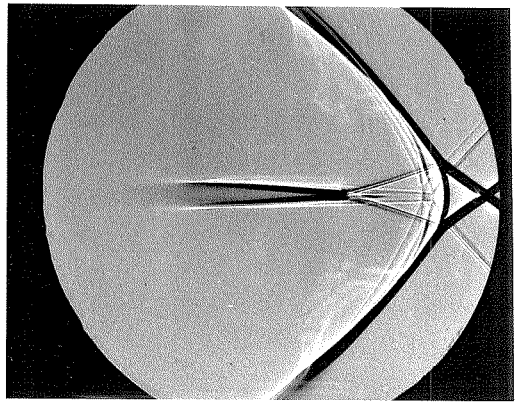

0.12

FIG. 31 SUCCESSIVE STAGES OF A WEAK SHOCK AT AN ARÊTE
(M_S = 1.2, REFLECTOR 6)

In the next picture (bottom row, on left), the shockfront has just passed the cusp. (The cusp refers to the cusp predicted by geometrical acoustics for this focussing situation.) In this case, the diffraction is seen more clearly. It has the form of a compression wave being followed by an expansion wave. In fact the compression appears to be forming into two small shock waves on the two sides of the shockfront. In the third picture (top row, on the right), these shock waves have grown bigger and are clearly distinguishable. They seem to form as very weak shocks, in the middle of the diffracted compression region, but closer to the reflected shockfront they become stronger (indicated by the variation in the thickness of the sharp, dark shadow). These shocks intersect with the shock, forming two three-shock intersections, with a common stem shock. In this case, strong refraction of light has masked the stem shock in the center, but its span is indicated by the separation between the two slipstreams of the two three-shock intersections (two pairs of dark and bright lines, trailing in the fluid). It must be emphasized, at this point, that the formation of the diffraction shocks (shocks formed from smooth diffraction waves) and the simultaneous formation of the three-shock intersections is inherently a nonlinear process. Thus these processes are very similar to those near a perfect focus.

The further development of this configuration of shocks is shown in the last picture of this sequence. The reflected shockfront has crossed ahead of the focussed shock, which appears to follow, thus forming a triangular loop in the shockfront. The diffraction shocks now meet the two off-axis apices of this triangle, making three-shock

intersections at those points. The slipstreams of these intersections have crossed in the fluid behind the shockfronts. This indicates that the three-shock intersections in picture three have met on the axis and have passed through each other. The slipstreams have thus bounded the dark peninsular region, which is the fluid heated by the strong stem shock. Qualitatively, the slipstreams indicate the paths of the intersections, or shock-shocks. Thus, in this case, nonlinear diffraction processes behind the shockfront lead to the formation of two shock-shocks. Then, the shock-shocks cross. At all points beyond their crossing, crossed and folded shockfronts are seen. This, again, is very similar to the perfect focus of a weak shock. The major difference occurs in the diffracted expansions behind the focussing shock. In this case, they are not distinct, with the result that the shock-shocks start far apart, and there is no distinct point marking the beginning of the focal spot (see Fig. 14, sec. 3.1).

Fig. 32 shows such shadowgraph sequences (rows, from left to right) for four different incident shock strengths. From the top three sequences, it is clear that with increasing shock strength, the focal region becomes larger and the triangular loop becomes smaller. Finally, as shown in the last sequence, the shock-shocks cannot cross, but simply spread apart, leaving a focal region of indefinite extent. The final shockfront is not crossed and the triangular loop has disappeared. This behavior is totally analogous to the shock wave behavior near perfect foci (see Fig. 16, sec. 3.1).

It is interesting to note that the slipstreams of the three-shock intersections in the last sequence of Fig. 32 become turbulent at a

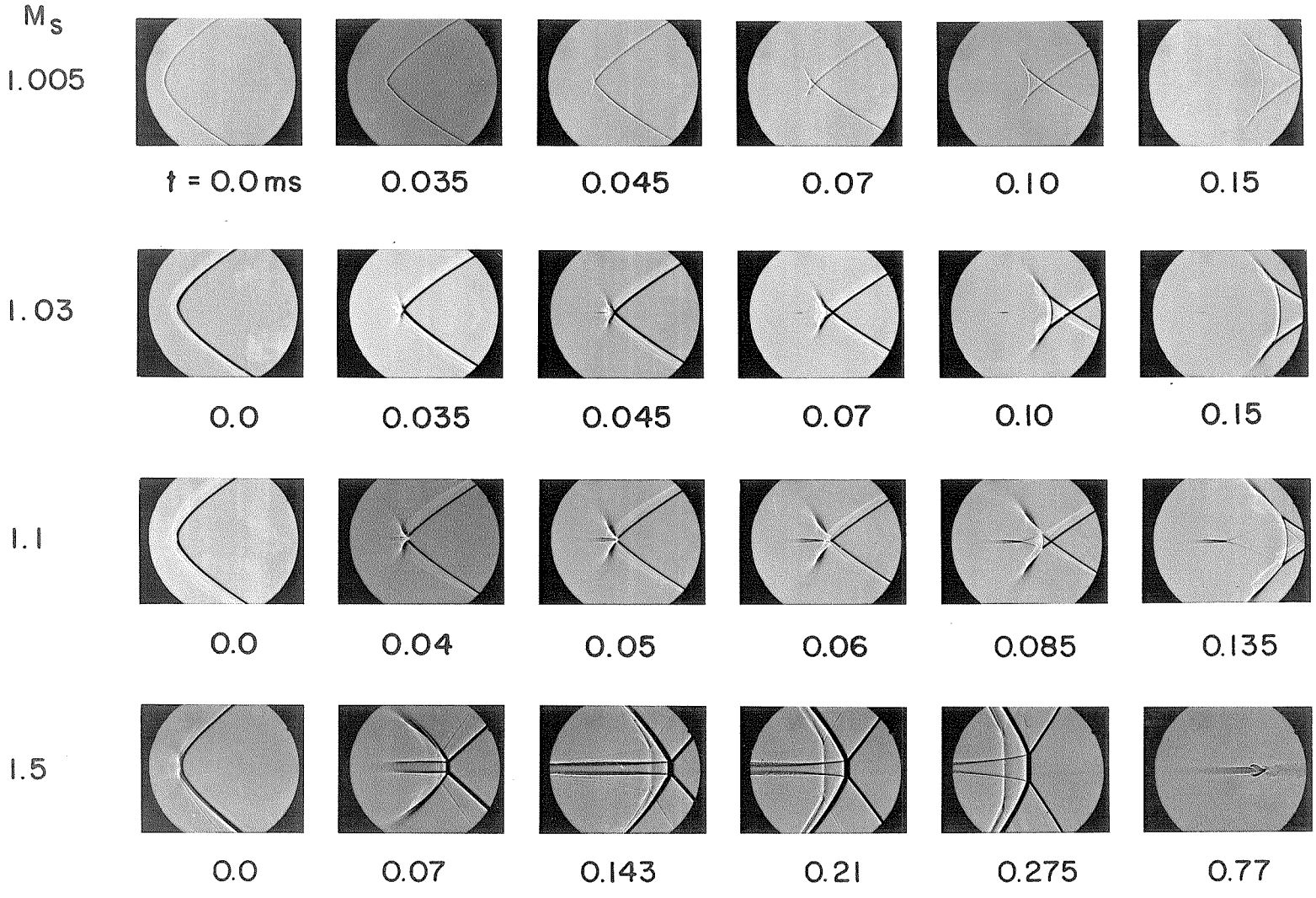

FIG. 32 EFFECT OF SHOCK STRENGTH ON AN ARÊTE (REFLECTOR 6)

short distance behind the intersections (pictures 3, 4 and 5). The last picture of the sequence shows the starting point of slipstreams. Being shear layers, they become unstable and roll into two line vortices. The layers beyond the vortices are turbulent and merge together to form a jet.

Similar to the case of perfect foci, it is possible to distinguish four kinds of behaviors near an arete; these correspond to sound pulses, weak shocks, moderately strong shocks and strong shocks, and are shown schematically in Figs. 33, 34, 35 and 36. The shock-shocks in each case are shown with a pair of dashed lines close to the axis of symmetry. The other pair of dashed lines (on the outside) mark the loci of the extremities of the diffraction shocks. In the acoustic limit they all coincide with the two branches of the caustic. With finite amplitude, the locus of the shock extremity shifts towards the center of curvature of the caustic, where as the shock-shocks shift away from it. Consequently the shock-shocks cross on the axis and form the narrow, peninsular focal region. The region between the shock extremity locus and the corresponding shock-shock is also inherently nonlinear and corresponds to the focal region of the caustic inside it. The arrows in the figure indicate the motion of the inflexion points of the shockfront. The angle enclosed by these lines represents the effective angle of convergence of the shockfront, in the case of an arete.

4.2 Pressure Waveforms for an Arete

Some typical pressure traces observed in the different regions of the flowfield are presented in Fig. 37. The line sketch schematically

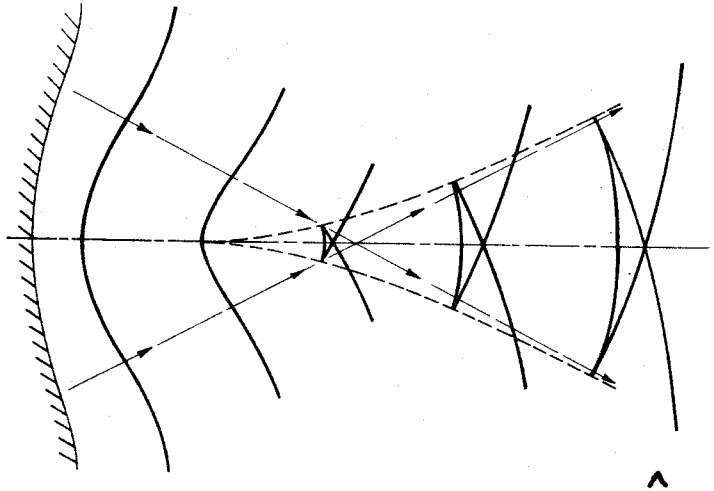

FIG. 33 SOUND PULSE AT AN ARÊTE

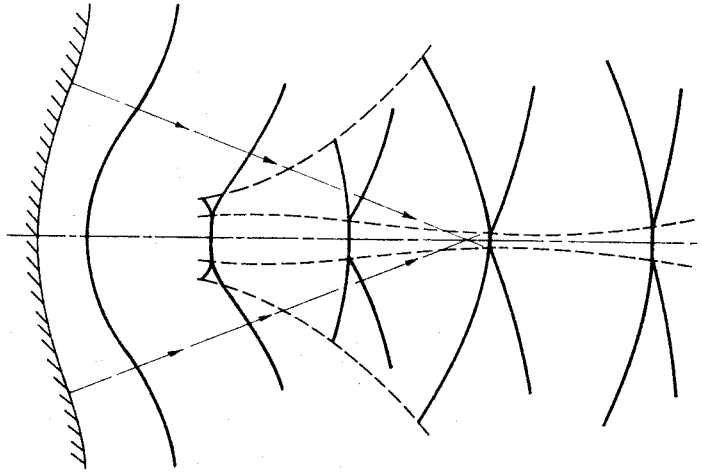

FIG. 35 MODERATELY STRONG SHOCK AT AN ARÊTE

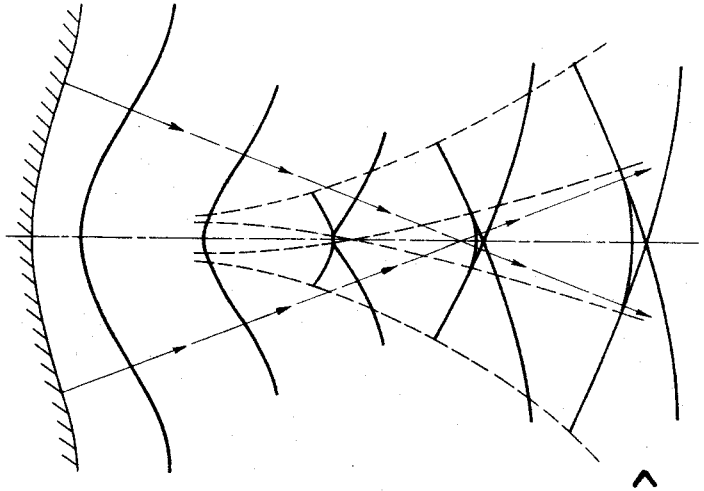

FIG. 34 WEAK SHOCK AT AN ARÊTE

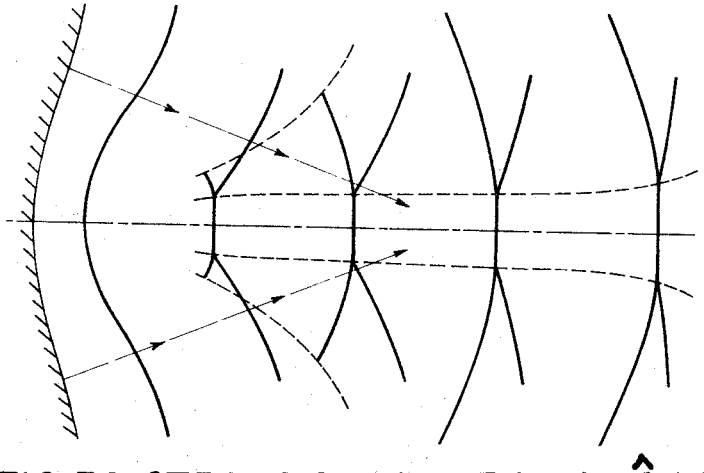

FIG. 36 STRONG SHOCK AT AN ARÊTE

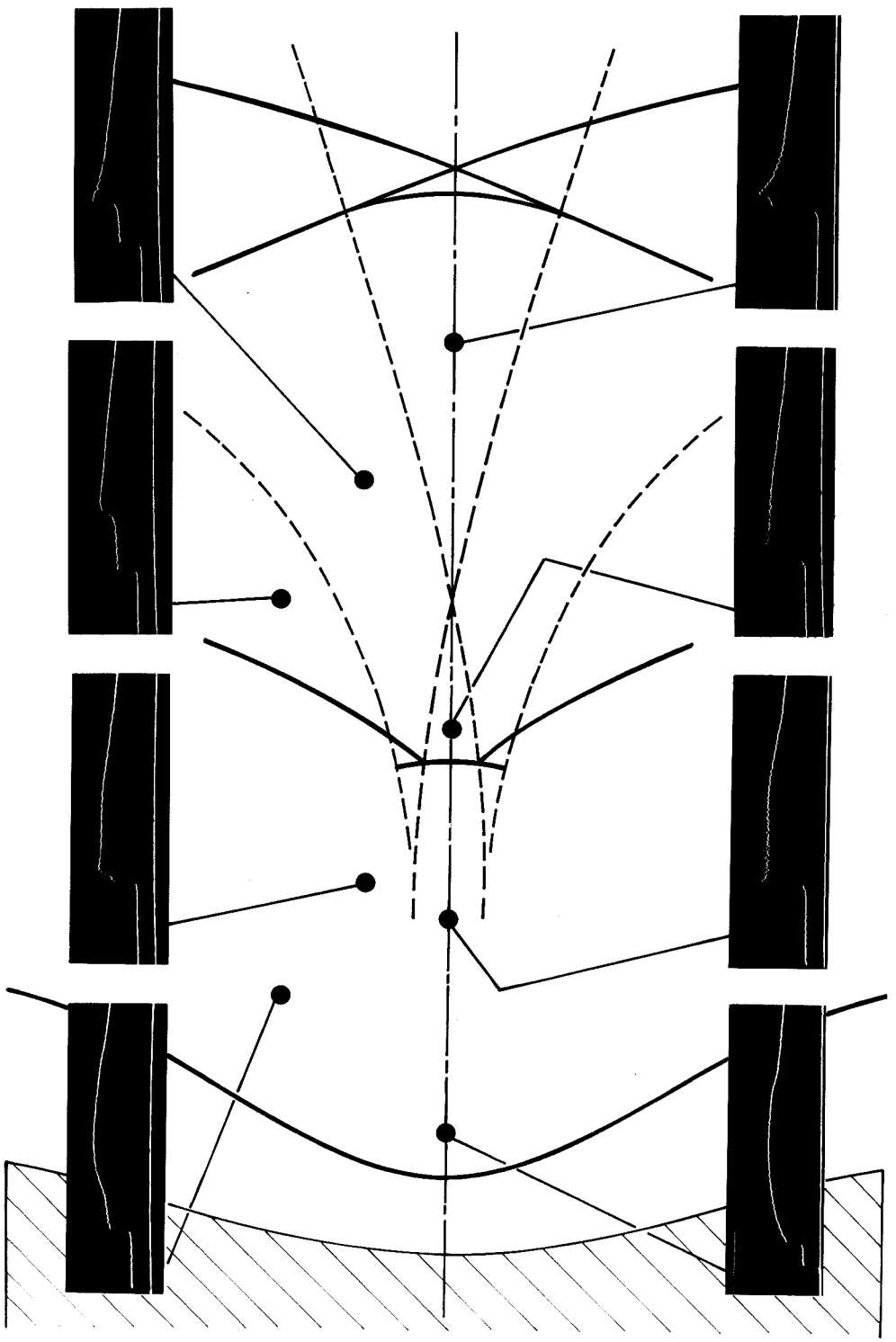

FIG. 37 PRESSURE TRACES FOR AN ARÊTE
(REFLECTOR 6, $M_s = 1.1$, 5.9 psi/cm, 50 μ sec/cm)

shows the focussing of a weak shock wave near an arete (cf. Fig. 34). The dark spots represent the points of measurement. The corresponding pressure histories are shown with indicators.

On the leftmost pressure traces the first pressure jump is the incident shock, which is followed by the reflected shock. Behind the reflected shock, effects of diffraction can be seen. To the left of the focal regions (of the cusp and of the caustic), the diffraction generally appears as a smooth compression, followed by a smooth expansion. The processes of importance, however, occur near the foci. Along the axis into the focal region, the waveform distorts in such a way that the shock jump is magnified greatly, but is immediately followed by a sharp expansion. (In the case of perfect foci also, a similar waveform occurs in the focal region.) Such a sharp expansion, due to nonlinearities, overtakes the shock and controls its amplitude in the focal region.

Near the focal region of the caustic, the smooth compressive diffraction (top row, trace 1) gradually steepens (top row, traces 2 and 3) and forms into the diffraction shock across this focal region (top row, trace 4). Again the diffracted expansion which follows the compression overtakes this shock in this region, as seen in the last trace. Thus, even in the case of a caustic, the maximum amplitude is controlled by nonlinear effects.

For strong shocks the focal region of the cusp extends to infinity and the last region of crossed and folded shockfronts does not occur. Then the wavefrom corresponding to the focal region of the cusp occurs all along. The other waveforms are similar for all shock

strengths.

Figs. 38 and 39 qualitatively show the nature of the pressure field in the two important focal regions, with isometric views. The wavefronts are shown in the ground plane (heavy lines, dashed where they lie under the pressure surface). Also the caustics and the shock-shocks are indicated. The wavefronts are moving towards and to the right of the observer. The line patterns drawn on the pressure surfaces (light lines) may be identified with the waveforms occurring at corresponding locations on the ground plane.

Fig. 38 shows the pressure field near the cusp of the caustic. The shock amplitude in the focal region is being controlled by an overtaking expansion. On both sides of the arete, this expansion blends into the expansion behind the smooth diffraction wave. The compressive part of this diffraction, however, gradually becomes steeper in regions closer to a focus. The formation of the diffraction shock with an extremity can now be visualized in terms of the nonlinear distortion of such a compression front.

As the shockfront approaches the crossing of the shock-shocks, the span of the stem shock tends to zero. This amounts to a simple modification in Fig. 38. Beyond the crossing of the shock-shocks, the focal region separates with the two branches of the caustics. The pressure surface also splits into two configurations joined by the crossed waves and the focussed shock (Fig. 37). The pressure field occurring near the left branch of the caustic (lower branch in Fig. 37) is shown in Fig. 39.

This pressure surface occurs near the focal region of a caustic.

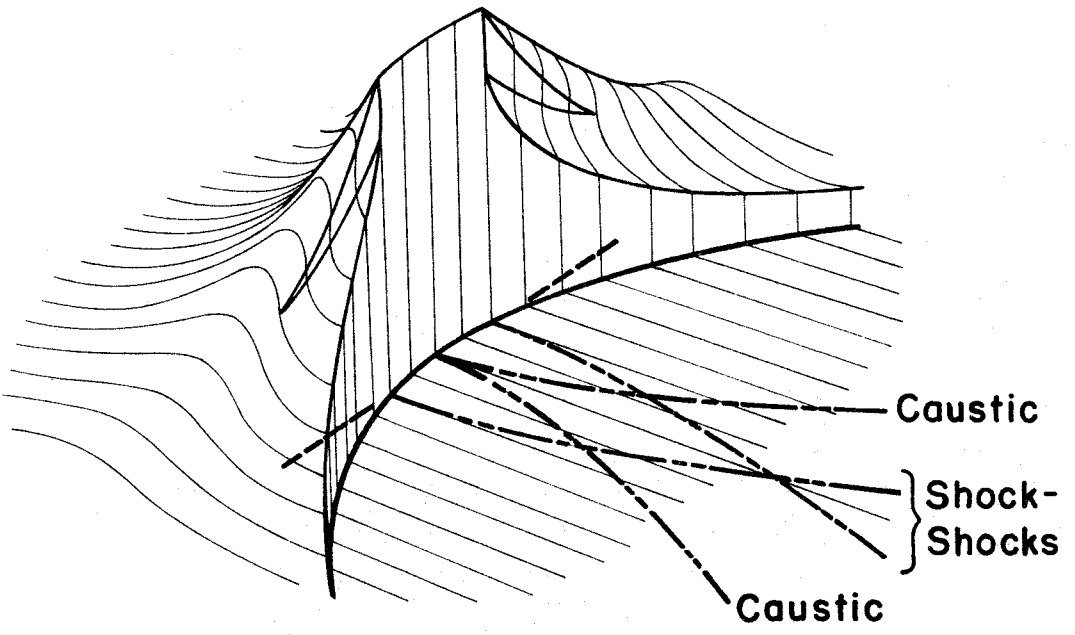

FIG. 38 PRESSURE FIELD AT AN ARÊTE

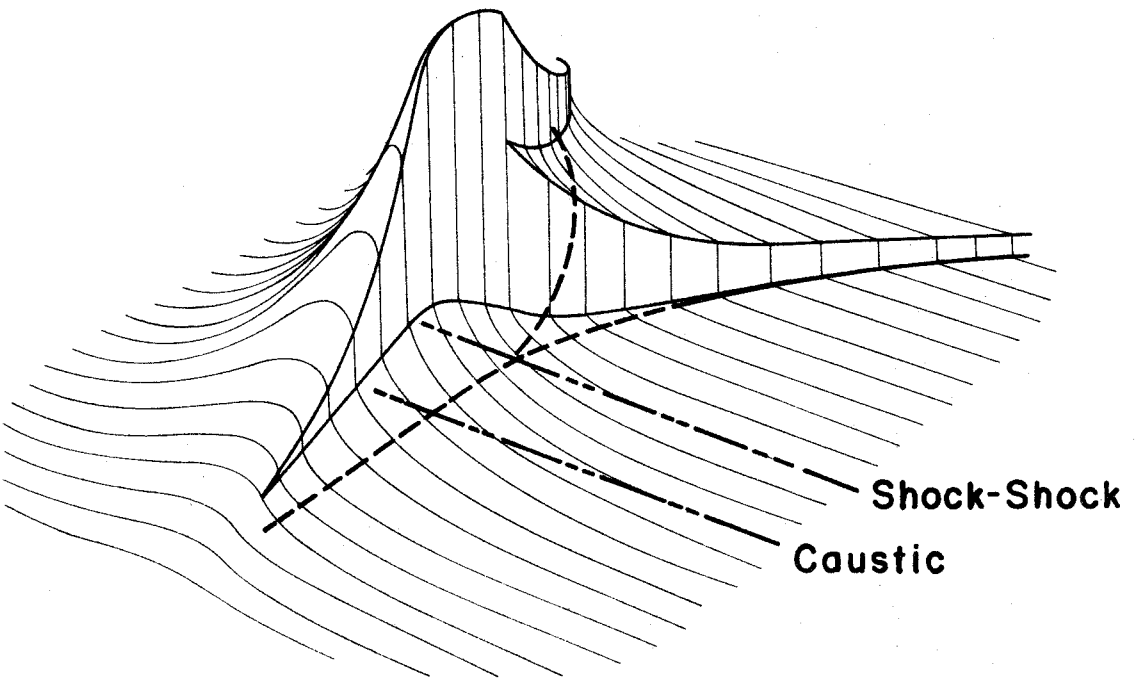

FIG. 39 PRESSURE FIELD AT A CAUSTIC

The diffraction waves associated with it correspond to the left half of the pressure surface in Fig. 38. The major difference occurs in the three shock intersection. In this case, the diffraction shock forms the stem shock of this intersection. The two other shocks are respectively the focussing shock and the focussed shock (see crossed and folded shockfront, Fig. 37).

It may be added that these pressure fields may be reduced to the predictions of acoustics, by removing the nonlinear effects.

4.3 Influence of Shock Strength

The shock-shocks and the distribution of peak amplitude exhibit the important features of the behavior of a shock wave near a cusped caustic. Therefore the influence of shock strength on the focussing process is briefly examined in terms of shock-shocks and peak amplitudes.

Fig. 40 shows the shock-shocks and the extremity loci (dashed) of the diffraction shock for one branch of the cusped caustic. The curves are traced from shadowgraphs for different incident shock strengths. For a given shock strength, the region between the corresponding shock-shock and the shock extremity locus represents the focal region of the caustic. The lateral growth of this region with increasing shock strength, and also along the caustic, is quite evident. This behavior is essentially the same as that of nonlinear distortion which increases with nonlinearity and distance traveled (sec. 1.3).

The region to the left of the intersection of the shock-shock with the axis represents the focal region of the cusp of the caustic. The three-shock intersections occurring on the shock-shocks can be

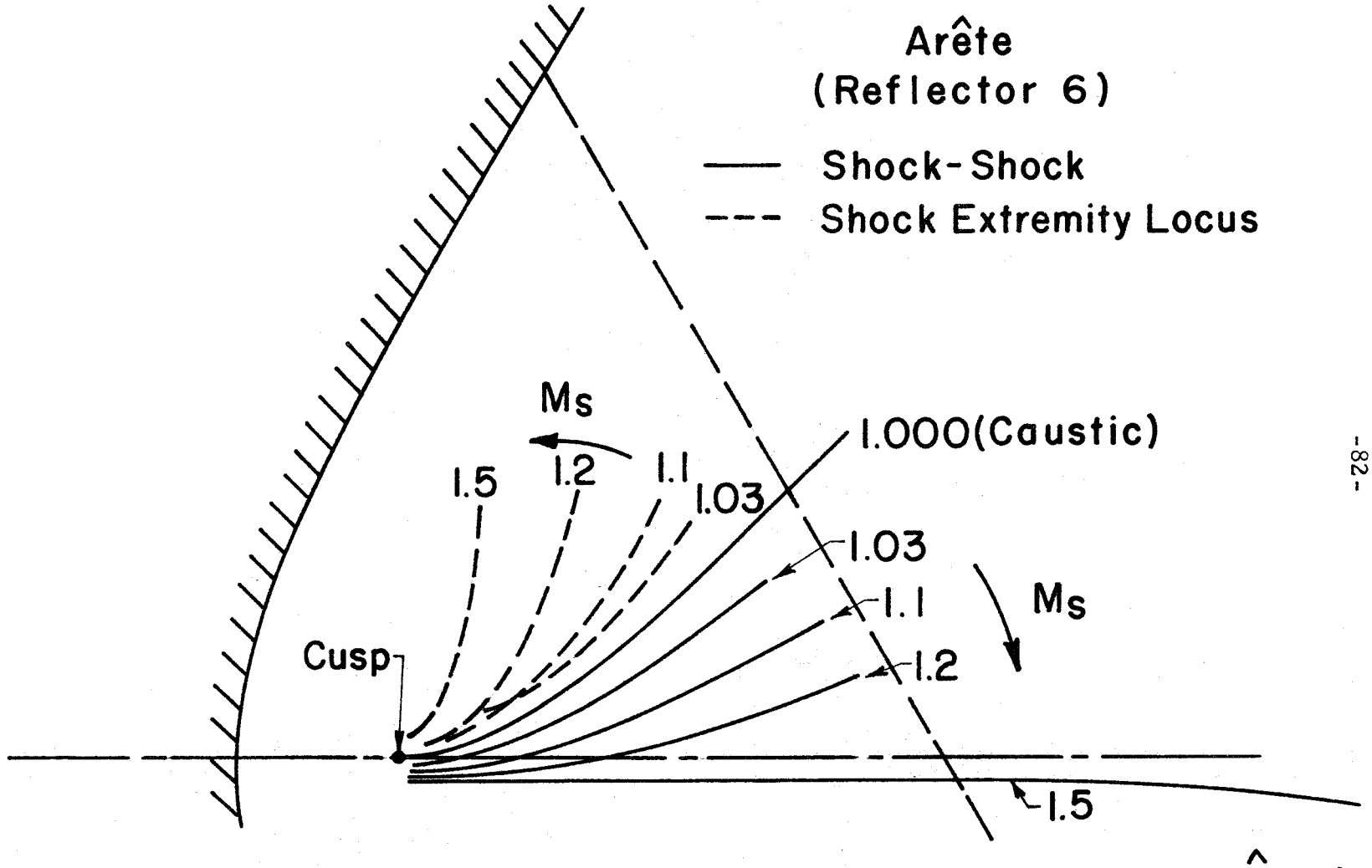

FIG.40 EFFECT OF SHOCK STRENGTH ON SHOCK-SHOCKS (ARÊTE)

compared with the "inverted" and the "direct" intersections (sec. 1.3). Their behavior in producing crossed shockfronts or uncrossed shockfronts is very parallel. This is the case, also near a perfect focus. (sec. 3.4).

The influence of shock strength on peak amplitudes along the axis is shown by Fig. 41. (All amplitudes in the reflection are normalized with the pressure jump across the normally reflected shock.) The curve for M = 1.1 shows that the shock amplitude (lower branch) is smaller than the peak amplitude before the arete. There is no well-defined starting point for the focal region of the arete. Also the point of maximum amplitude does not appear to correlate with some other specific feature of the flow, except that it occurs within this focal region. This is due to the smoothness of the diffraction waves. Further, the end of the focal region is not marked by any significant change in the variation of peak amplitude.

However, the most important fact is that the maximum amplitude is smaller for larger shock strengths. This indicates that, though the processes near an arete are not as well defined as near a perfect focus, the amplitudes are still controlled by the nonlinear mechanism, in which a sharp expansion overtakes the shock and reduces its amplitude.

4.4 Smooth Caustic

A "smooth" caustic, as used here, implies a caustic with a constant radius of curvature. Not only does this distinguish a smooth caustic from an arete, but as explained in sec. 1.1, it qualifies the caustic to be a steady caustic in the approximation of geometrical

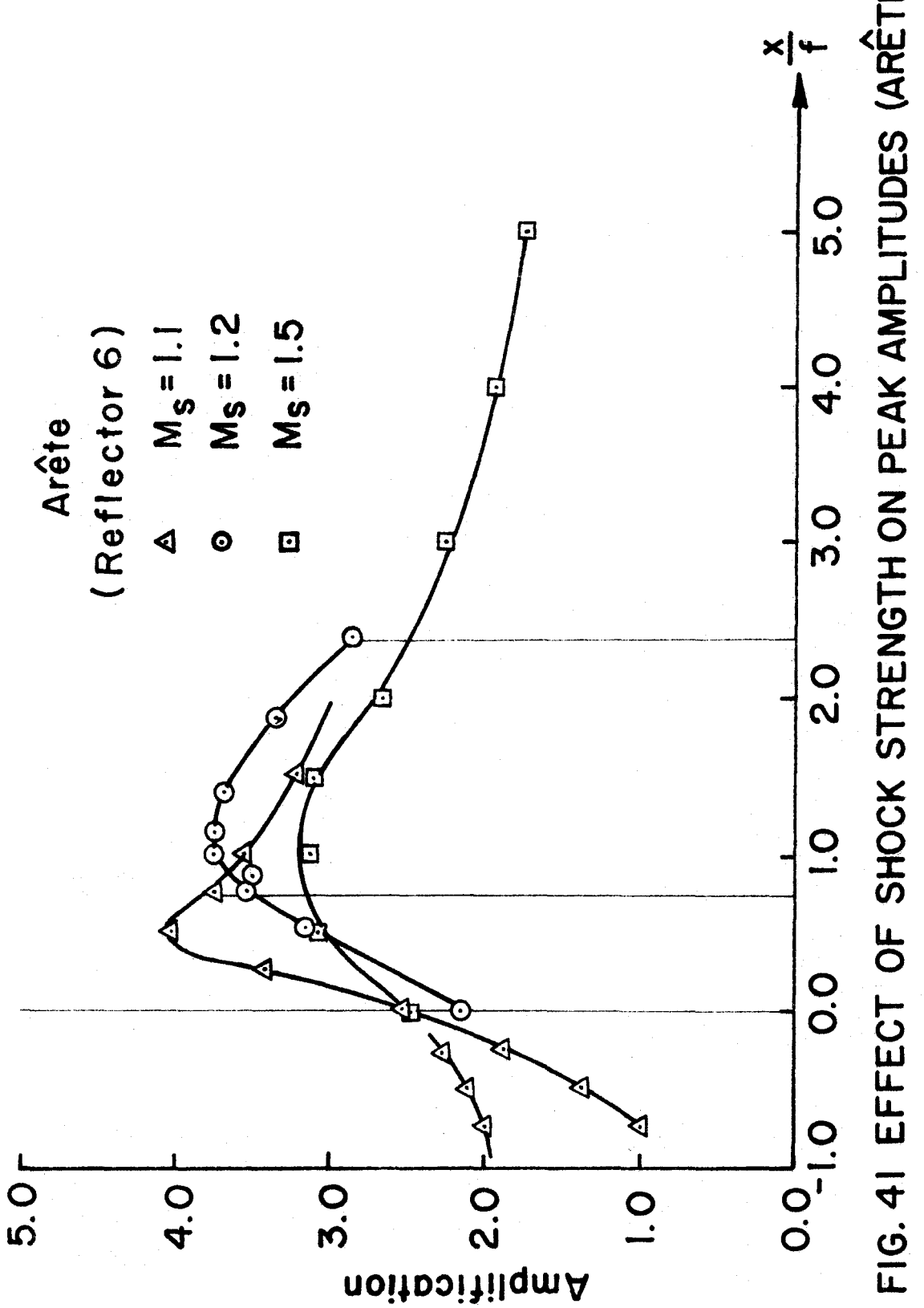

FIG. 41 EFFECT OF SHOCK STRENGTH ON PEAK AMPLITUDES (ARÊTE)

acoustics.

Fig. 42 shows shadowgraphs of shock waves at successive points (to the right) along the caustic for two different shock strengths (two rows). The caustic is an arc of a circle, convex downwards, in the upper part of the picture. In the first picture for the weak shock (top row), the reflected shockfront has just started to cross. This process is essential at the starting point of a caustic (sec. 1.1). The wave behind the shockfront (on the left), is a diffracted expansion due to the discontinuity in the radius of curvature of the shock. This also is an essential feature of the starting point. The next picture shows the crossed and folded front. The triangular loop so formed has its upper apex traveling along the caustic. The next picture shows the cross and the other fold of the loop moving away, giving the caustic an appearance of a steady caustic. Details of the focal region are not distinguishable in these pictures, however, the shock does end near the caustic. Also some amplification of the shock due to focussing is observable (the width and darkness of the shadow of the shock increases towards the caustic).

For a stronger shock (bottom row), the details of both the initial crossing and the focal region of the caustic can be seen more clearly. In the first picture a smooth diffraction front is seen on the concave side of the caustic (upwards), which has steepened into a diffraction shock forming a three-shock intersection with the compressive diffraction as indicated by the slipstream (upper). The diffracted expansion also shows a shock ahead of it, forming another three-shock intersection and another slipstream (lower). It is interesting to note

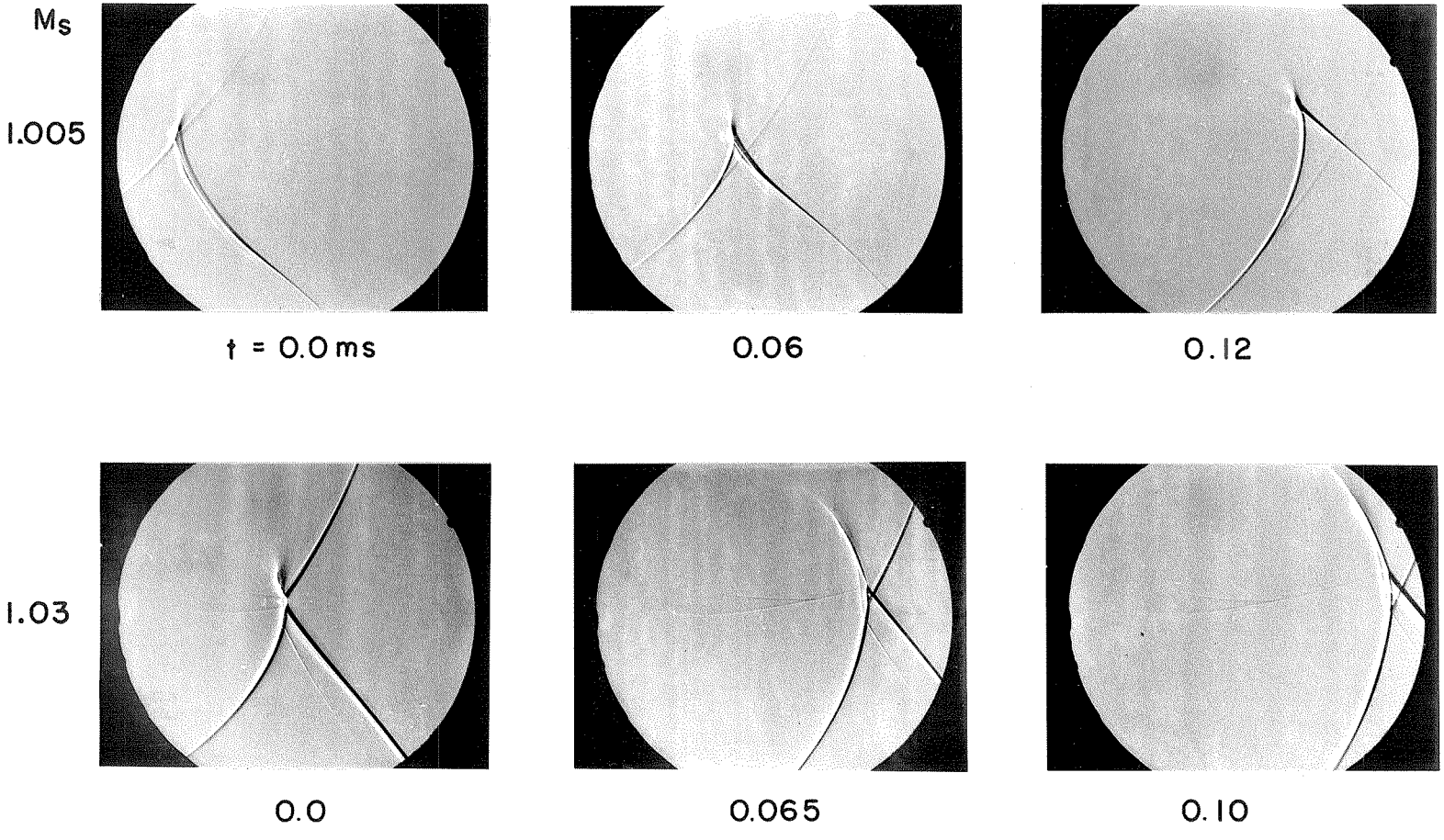

FIG. 42 EFFECT OF SHOCK STRENGTH ON A SMOOTH CAUSTIC (REFLECTOR 5)

that at this stage, the upper part of this focus is comparable to an arete, whereas the lower part is comparable to a perfect focus. The next stages show the subsequent crossing of the shockfront, and the growth of the focal region of the caustic. Figs. 43 and 44 show this behavior schematically, for a sound pulse and for a weak shock. The formation of a diffraction shock and the two shock-shocks, in the weak shock case, is clearly a nonlinear process.

The growth in time of the diffraction shock out of the smooth diffraction indicates that the caustic is not steady. This nonsteadiness is associated with the method of producing the caustic. At points further down the caustic, the distance traveled by the focussing shock-front is larger (since reflection), and correspondingly, the nonlinear distortion is larger. This implies that the nonsteadiness is not inherent, and occurs because the nonlinear phenomena near the focus scale with the initial radius of curvature, which varies along the reflected shockfront in this case.

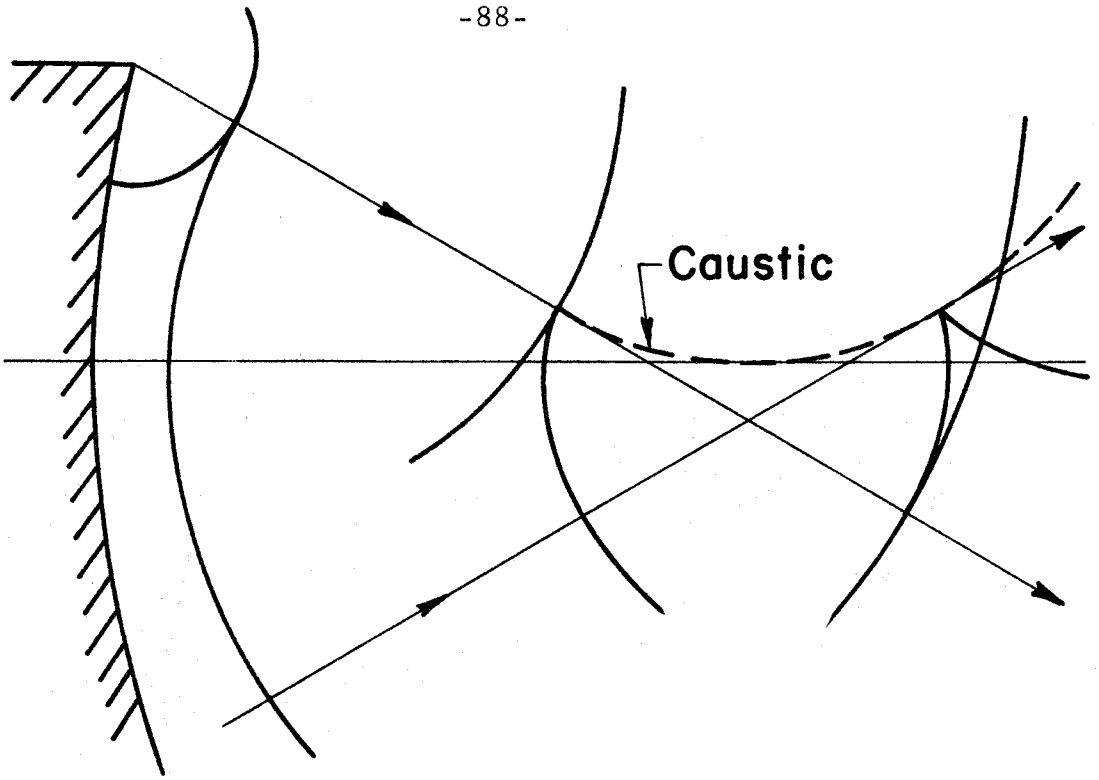

FIG. 43 SOUND PULSE AT A SMOOTH CAUSTIC

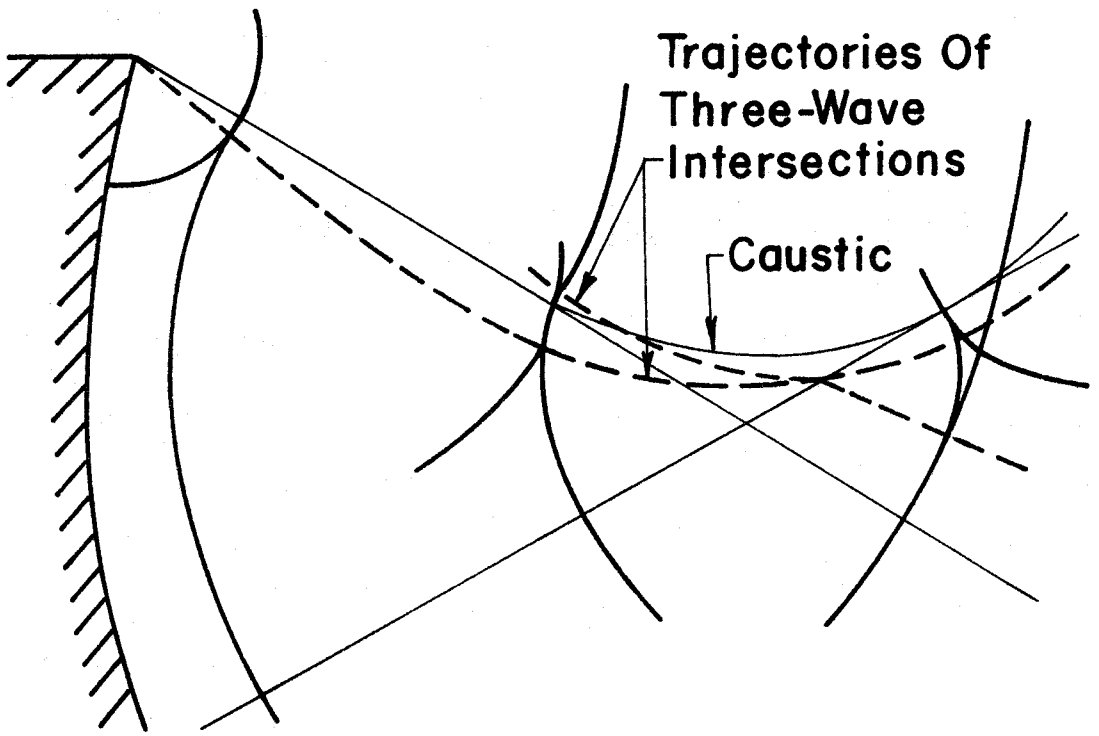

FIG. 44 WEAK SHOCK AT A SMOOTH CAUSTIC

V. CONCLUSION

This chapter summarizes the observed phenomena and their interpretations in more general terms. First the essential features of the observed nonlinear behavior of focussing weak shock waves are described. Then the important focal processes are discussed in relation to acoustic and nonlinear behavior of shock waves.

5.1 Nonlinear Focussing of Shock Waves

Shadowgraphs of various stages of different shock-focussing situations have shown the influence of shock strength and angle of convergence on the geometry of focussing shockfronts.

For weak shocks, the shockfront coming out of the focus is crossed and folded, forming a triangular loop, in qualitative agreement with acoustics. However, very minor distortion of the geometry of the fronts does occur. This leads to prominent changes in the wavefronts near the focus; three-shock intersections form (essentially, a nonlinear process), and their paths delineate a focal region. The shockfront is this region is almost plane and normal. Further down, the three-shock intersections pass through each other and terminate the focal region; beyond this point, a crossed shockfront is seen.

For stronger shocks, the distortion in the geometry increases, leading to larger focal regions and smaller loops on crossed shockfronts. For some critical shock strength a transition occurs in the geometry of the shockfronts. Then, the three-shock intersections do not pass through each other, the focal region extends to infinity, and the shockfront coming out of the focus is uncrossed and has no loop.

The amplitude dependence of these phenomena and their

geometrical character indicates that they are manifestations of nonlinear distortion of the wavefield. Further, the distortion is more effective in modifying and transforming wavefronts if the geometry is shallow. In other words, rapid convergence of waves suppresses the effects of nonlinear distortion, and for shallow shockfronts the nonlinear effects begin to dominate the focussing at very weak shock strengths.

Pressure histories recorded at various locations, for some of the shock-focussing situations mentioned above, show the character of the different fronts and indicate the diffraction processes occurring between the fronts (not seen in the shadowgraphs).

The basic character of the observed diffraction effects behind the focussing shockfronts is consistent with acoustics. Nonuniformities of shock strength along the shockfront create diffraction waves and eliminate nonuniformities of pressure in the flow behind; compressions travel into regions of low pressure, whereas expansions travel into regions of high pressure.

Thus, the focussing (and therefore amplifying) shock wave is followed by strong expansion waves, whereas it sends compression waves into the fluid behind weaker shocks. The nonlinear behavior of these finite amplitude waves leads to two important effects:

1. The compression waves distort and break into shocks, which intersect with the shockfront to form three-shock intersections.

2. The expansion waves overtake the amplifying shock before it goes to a focus and reduce its amplitude in the focal region. This nonlinear effect is responsible for limiting the maximum amplitude.

Furthermore, for stronger shocks, the expansion overtakes the shock earlier. Therefore, the maximum pressure amplification near the focus is smaller for stronger shock waves.

In summary, the nonlinear distortion processes in the wavefield behind the focussing shock modify the shock, resulting in geometrical distortion of the shockfront. In particular, nonlinear diffraction is responsible for determining the focal region and the maximum amplitude near the focus.

5.2 Focal Processes

Diffraction in the wavefield behind the shock plays a major role in both nonlinear focussing and acoustic focussing of thick shocks (sec. 1.2c). In both cases it interacts with the focussing shock, and controls the amplitude in the foci, essentially by distributing the wave energy concentrated by focussing, in a small region along the shock. The plane normal shock in the nonlinear focal region and the locally plane fronts of an acoustic focus (sec. 1.2c) are examples of such interactions.

In nonlinear focussing, the length by which the wavefield has overtaken the shock is a scale of the extent of the interaction, whereas in acoustic focussing the shock thickness is the measure for an overlap region between the shock and the diffraction field. Therefore, in a given situation, the dominating lengthscale of the two determines the size of the focal region and the kind of focussing. Since for weaker shocks, nonlinear distortion is smaller and the shock thickness is larger, a transition from nonlinear focussing to acoustic focussing is expected as the shock strength gets very small.

Even though the control of amplitude near the focus is largely attributed to diffraction effects, viscosity and other dissipative mechanisms also are crucial to the process in an indirect manner. These mechanisms are primarily active within the shock thickness. In acoustic focussing, they determine the shock thickness, which leads to finite amplitudes in the focus. However, this effect is primarily due to such dissipation occurring throughout the fluid, and not necessarily only at the focus. As compared to this, in nonlinear focussing, the prominent dissipative effects are quite local, such as heating of the fluid in the focal region. In this case, the dissipation of the wave energy at the shock is directly controlled by nonlinear effects, which become prominent near the focus. However, it must be emphasized that for such weak shock waves the dissipation is only a small fraction of the total energy in the wave.

It is also possible that the three-shock intersections and their slipstreams have a structure much larger than the shock thickness due to viscosity (Sternberg, 1959). This may become important in the small focal regions of weak shock waves.

In general, diffraction and viscous dissipation are both important processes that control the maximum amplitude near the focus. The invariance of wavespeed in acoustic focussing restricts their action on the amplitudes. On the other hand, with finite amplitudes, the nonlinear increase in wavespeed and the consequent distortion of the wavefield greatly enhance the influence of these processes and result in reduced maximum amplifications near the foci.

REFERENCES

Sternberg, J. 1959 Triple-Shock-Wave Intersections, Phys. of Fluids 2 (2), 179.

APPENDIX A

APPROXIMATIONS IN THE NUMERICAL SIMULATION OF THE THREE-WAVE INTERSECTION TRAJECTORIES

Trajectories of three-wave intersections represent the important geometrical aspects of the behavior of focussing shockfronts. This appendix describes a method for numerically simulating the trajectories in the case of a perfect focus. The essential behavior can be qualitatively simulated by modeling the nonlinear increase in the wavespeeds of the intersecting fronts. Other effects, linear or nonlinear (such as diffraction and its effect on the shockfront), are crudely approximated to improve the simulation.

If the shock ahead of the intersecting wave has a Mach number M (Fig. 45), then the intersecting wave is assumed to have a speed $a_0(2M-1)$ independent of its amplitude and direction. (a_0 is the speed of sound in the fluid ahead of the shock.) Further, if the angle α is known, the angle β can be found as a function of M and α, which completely determines the motion of the intersection in this approximation. The intersection travels upward along the incoming shockfront ($\beta - \alpha < \pi/2$, if $M > 1$), which is the nonlinear effect primarily responsible for the observed behavior of the trajectories.

When an intersection travels on a converging shockfront, α and consequently β tend to become large, which produces another effect. The shockfront which is moving almost as rapidly as the intersecting wave, casts a "shadow" in the intersecting wave, and the intersecting wave diffracts into this shadow. (The shadow occurs because the portion of the wavefront already merged with the shock cannot separate from

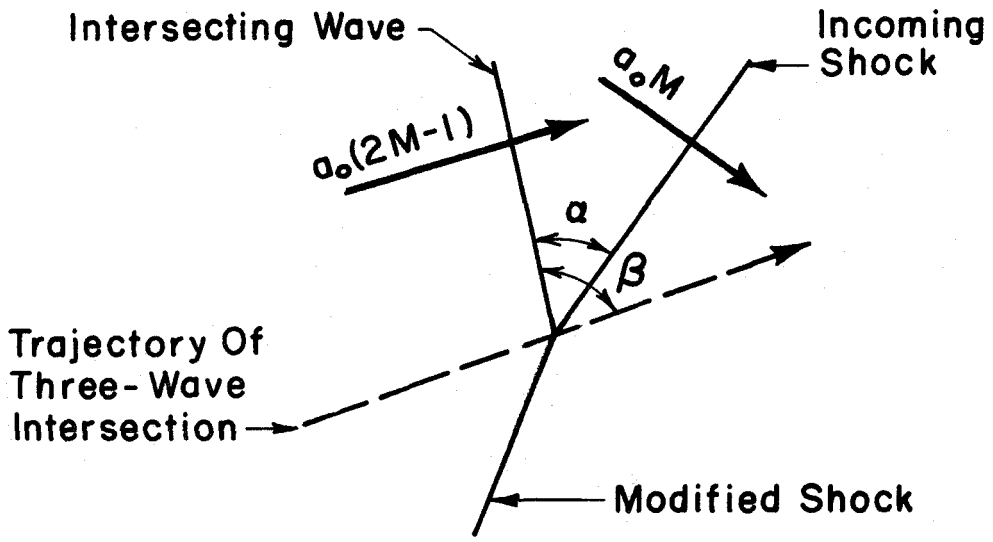

FIG. 45 A THREE-WAVE INTERSECTION

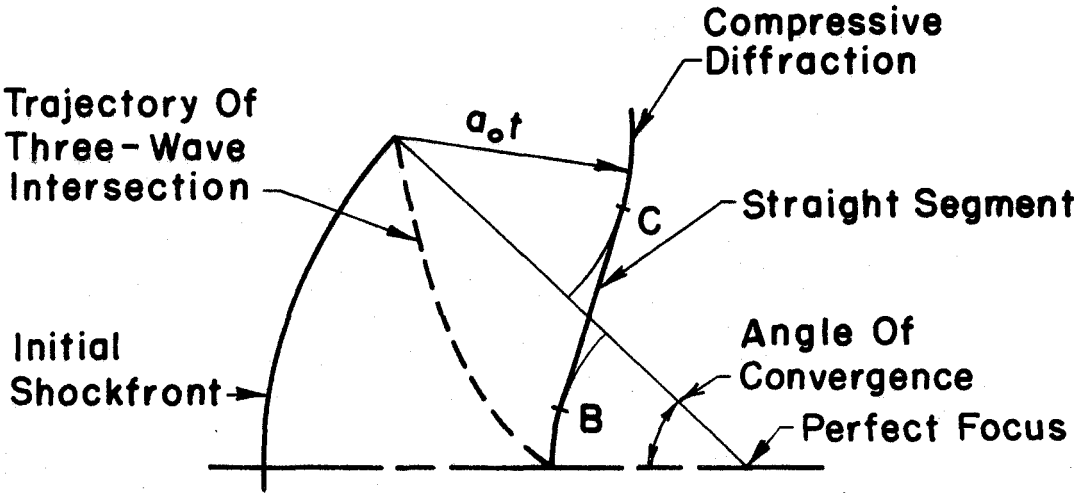

FIG. 46 APPROXIMATE SHOCKFRONT

the shock.) The diffraction curves the intersecting wavefront, continuously re-orients the intersection and limits the maximum value of β. (In Fig. 15, the high curvature of the diffracted expansion front, close behind the converging shock, is evidence of such diffraction.) The maximum value of β is taken to be $\pi/2$ in this calculation. The corresponding α is a maximum for a given M. Due to this effect, the local curvatures of the shockfront and the trajectory are quite similar. Further, the speed of the intersection along the shock is a minimum and depends on M alone. The latter result is parallel to the speed of a wave on the shock along the shock (sec. 1.3).

Thus, for a shockfront with a perfect focus, two intersections occur at the two reflector corners and travel towards the center. The segment of the shock between them is assumed to be circular and its strength is predicted according to acoustics. This determines the trajectories to the point where they meet on the axis.

When the two intersections meet, the whole shockfront has been affected by them, and its shape and strength are not known and must be assumed in order to continue the calculation. Most approximate forms for these quantities lead to qualitatively identical results. The approximations that produced the best simulation in these computations are outlined below.

The diffracted compression fronts from the reflector corners are assumed to have zero shock strength. These fronts travel with speed a_o. This results in a misfit between this diffraction front and the converging shock (Fig. 46). The misfit is eliminated by assuming that, in this region, the shockfront is a straight line tangent to the two

fronts. This approximation is based on the shapes of shockfronts observed in Figs. 15 and 16.

The distribution of shock strength on this shockfront is expected to follow the trends shown in Fig. 22 (the shock-jump variation along the diffraction-affected shockfront, before focus). Such a distribution is simulated with the following assumptions. The shock strength has its maximum value at point A as predicted by acoustics (Fig. 46). The shock strength falls exponentially along the converging shockfront and reaches its half value at point B. (This is partially justified because, in the diffraction field behind a discontinuity in the amplitude of an acoustic shock, the amplitude is the mean of the amplitudes across the discontinuity.) Along the straight shock segment it varies linearly and becomes zero at point C.

It is possible to continue the computation with the above approximations for the shape and strength of the shockfront. The good agreement obtained between the results and the observations suggests that the errors introduced by the approximations are small. In other words, the results are not very sensitive to such crude approximations.

TABLE I

CONDITIONS FOR PRODUCING VARIOUS SHOCKS

IN THE GALCIT 17" SHOCK TUBE

M_s	Diaphragm		P_1 atm
	material	thickness (in inches)	
1.005	Mylar	.00025	1.0
1.01	"	.0005	1.0
1.02	"	.001	1.0
1.03	Al 1100-0	.003	1.0
1.1	"	.006	1.0
1.2	"	.01	.67
1.3	"	.02	.67
1.5	"	.02	.33

Note: #1 set of crossed straight knife-blades was used.

TABLE 2

REFLECTORS AND THEIR CHARACTERISTICS

Reflector			Reflection		
No.	shape	width (in inches)	focus	R_{min} (in inches)	Angle of Convergence
1	parabolic cylinder	8.0	perfect line focus	2.375	160°
2	"	"	"	4.75	90°
3	"	"	"	9.5	48°
4	axisymmetric paraboloid	8.0	perfect point focus	2.375	160°
5	asymmetric concave	9.25	caustic with 3.25" R	2.66	100°
6	concave with flat ends	8.5	arete	1.00	120°

Note: All reflectors had sharp edges, except the last reflector, which gradually became convex and filled the whole cross section of the tube. The first reflector was used also mounted in a flat baffle and in a smooth rounded baffle (see sec. 3.6). The last reflector was designed to produce an acoustic reflection of a shape $x = (0.5)y^2 - (0.01215)y^4$ (in inches).

TABLE 3

CRITICAL SHOCK STRENGTHS FOR TRANSITION IN THE GEOMETRY OF THE SHOCKFRONT

OBSERVATIONS					COMPUTATIONS	
No.	Type of Focus	f_{min} (in inches)	Angle of Convergence	M_t (value or range)	M_t (value or range)	Angle of Convergence
1	perfect line focus	2.375	160°	1.2	1.22	160.3°
2	perfect line focus	4.75	91°	1.03 - 1.1	1.05 - 1.075	91.5°
3	perfect line focus	9.5	48°	1.01 - 1.02	1.01 - 1.02	45.7°
4	perfect point focus	2.375	160°	1.1 - 1.2		
5	smooth caustic	2.66	100°	not measured		
6	cusped caustic (arete)	1.00	120°	1.3 - 1.5		